

This is an Open Access document downloaded from ORCA, Cardiff University's institutional repository: <https://orca.cardiff.ac.uk/id/eprint/144929/>

This is the author's version of a work that was submitted to / accepted for publication.

Citation for final published version:

Loza Espejel, Roberto , Alves, Tiago M. and Caçador Martins?Ferreira, Marco Antonio 2021. Depositional and geomorphic patterns of mixed calciclastic-siliciclastic systems on a deep-water Equatorial Margin. Basin Research 33 (6) , pp. 3321-3347. 10.1111/bre.12604

Publishers page: <http://dx.doi.org/10.1111/bre.12604>

Please note:

Changes made as a result of publishing processes such as copy-editing, formatting and page numbers may not be reflected in this version. For the definitive version of this publication, please refer to the published source. You are advised to consult the publisher's version if you wish to cite this paper.

This version is being made available in accordance with publisher policies. See <http://orca.cf.ac.uk/policies.html> for usage policies. Copyright and moral rights for publications made available in ORCA are retained by the copyright holders.



Depositional and geomorphic patterns of mixed calciclastic-siliciclastic systems on a deep-water Equatorial Margin

Roberto Loza Espejel^{a,*}, Tiago M. Alves^a and Marco Antonio Caçador Martins-Ferreira^b

^a3D Seismic Lab, School of Earth and Environmental Sciences, Cardiff University, Main Building – Park Place,
CF10 3AT, Cardiff, United Kingdom

^bFaculdade de Ciências e Tecnologia, Universidade Federal de Goiás, Conde dos Arcos, 74968755, Aparecida de
Goiânia, GO, Brazil

*Corresponding author:

Mobile phone: +44 7479 746160.

E-mail address: lozaespejelr@cardiff.ac.uk and lozaespejelr@gmail.com

Keywords: *Equatorial Brazil; carbonate shelf; channel-levee systems; calciclastic
depositional systems; deep-water basins*

ABSTRACT

Distal slope and basin depositional systems in deep waters of the Pará-Maranhão Basin, Equatorial Brazil, are investigated using a high-resolution 3D seismic volume, borehole data and multispectral satellite imagery. A Neogene calciclastic submarine fan and a series of channel-levee systems are analysed at water depths of 100 m to 3,500 m. Channel-levee systems have sinuous and straight morphologies and are of different sizes. Their origin is related to turbidity flows sourced and funnelled from the carbonate shelf to submarine canyons and gullies, as well as from areas with marked slope instability. A mixed calciclastic-siliciclastic sediment input is recognised with autochthonous calcarenites and calcilutites comprising the bulk of sediment on the mid and outer continental shelf. Minor amounts of siliciclastic sediment sourced from small rivers occur on the inner shelf. Sedimentation processes of a distally steepened carbonate ramp are discussed considering a general depositional setting dominated by fluctuations in relative sea level. Cross-sectional and planar

parameters of mixed calciclastic-siliciclastic channel-levee systems are compared to their siliciclastic counterparts. Morphological results show similarities between calciclastic and siliciclastic channel-levee systems. As a corollary, three types of channel-levee systems are described: (1) channels related to calciclastic submarine fans, (2) low-sinuosity, aggradational channels, and (3) high-sinuosity channels.

1 Introduction

Deep-water channel-levee systems develop beyond continental shelves (Lemay et al., 2020), where sediment is transported from shallow waters into deep and ultra-deep water basins; described by Pettingill (2006) as ranging in depth from 500 m to 2,000 m, and extending beyond 2,000 m, respectively. Research on siliciclastic depositional systems has been generally the centre of attention in deep-water basins, with studies on calciclastic systems lagging behind the latter (Payros and Pujalte, 2008). Furthermore, when compared to carbonate-platform settings, deep-water carbonate systems are also less documented and poorly understood (Playton et al., 2010). Yet, deep-water calciclastic systems have recently regained interest in industry and academia due to the need of integrating deep-water deposits in global and local models of carbonate depositional systems. Such models are crucial as new hydrocarbon exploration plays are being sought beyond the more-common shallow carbonate depositional settings (Reijmer et al., 2015a).

Deep-water carbonate systems are key to understand the growth, evolution and depositional conditions of carbonate systems as a whole, and can be used to document the relationship between basin and platform settings (Playton et al., 2010). In fact, calcium carbonate (CaCO_3) is a significant source of sediment to the present-day ocean with an estimated discharge of about 5 billion tons (bt) per year, of which 3bt accumulate in sediments,

and the other 40% is dissolved (Milliman, 1993; Jorjy et al., 2020). Deep-water carbonate depositional systems (i.e. carbonate slopes and basins) can be categorised and subdivided based on their type of deposit, large-scale stratal patterns, and spatial architecture. Playton et al. (2010) grouped deep-water carbonate systems taking into account their dominant type of deposit: debris, grain- and mud-dominated. Spatial architecture in these settings are documented by Playton et al. (2010) and range from strike-continuous aprons to discontinuous tongues and channel-fan complexes. Calciclastic submarine fans and channel-levee systems are particularly less documented than slope aprons; they have been largely overlooked as they were, thus far, thought to be rare in the stratigraphic record (Payros et al., 2007; Payros and Pujalte, 2008; Back and Reuning, 2015; Dunlap et al., 2018).

Published work aiming to understand deep-water carbonate depositional systems include vintage articles with initial descriptions of carbonate slopes (e.g. Ditty et al., 1977; James and Mountjoy, 1983; Ravenne et al., 1985; Kenter, 1990; Coniglio and Dix, 1992), important compilations (Payros and Pujalte, 2008; Playton et al., 2010; Reijmer et al., 2015a) and recent studies in which depositional models separate carbonate settings from their siliciclastic counterparts (Mulder et al., 2014; Counts et al., 2019; Moscardelli et al., 2019; Jorjy et al., 2020). For instance, the modern and ancient Bahamian sedimentary system has been crucial to understand carbonate platform-to-basin sedimentation patterns, and recognise that carbonate-lobe and channel systems are able to develop in deep-water basins (Bornhold and Pilkey, 1971; Crevello and Schlager, 1980; Eberli et al., 1997, 2005; Betzler et al., 1999, 2014; Mulder et al., 2012, 2014; Reijmer et al., 2015a; Wunsch et al., 2017). Ancient outcrop examples have also been used to document calciclastic systems such as the Miocene Azagador Formation in southern Spain (Braga et al., 2001), the Eocene Anotz Formation in the western Pyrenees (Payros et al., 2007), and the Miocene Albacore slope fan in SE Australia (Gallagher et al., 2001).

New investigations based on high-quality seismic data have increased our knowledge of deep-water carbonates in areas such as the Browse Basin, Northwest Shelf of Australia, with carbonate deep-water channel-levee systems having been reported in Miocene strata (Back and Reuning, 2015; Rankey, 2017; Dunlap et al., 2018; Janson et al., 2018; Rinke-Hardekopf et al., 2018; Tesch et al., 2018; Zeng, 2020). In addition, Mulder et al (2014) and Wunsch et al. (2017) described a modern channel-levee system in the pure carbonate setting of the Bahamas Archipelago. Ultra-deep-water carbonate deposits are relatively less documented, but recent investigations have pointed out their existence in the form of channel-levee complexes and turbiditic lobes at water depths of 2,000 m to 3,400 m around isolated carbonate platforms in the Indian Ocean (Counts et al., 2019; Jorjy et al., 2020). Despite these efforts, geomorphological and architectural features of mixed carbonate-siliciclastic systems remain underexplored in the literature, possibly due to incomplete datasets leading to simplistic descriptions (Moscardelli et al., 2019). Mixed calciclastic-siliciclastic systems derive from the interaction between a siliciclastic source (usually river discharge) and a regional carbonate factory (Chiarella et al., 2017). These systems have been studied since the 1970s in regions such as the Hispaniola-Caicos Basin, where siliciclastic and carbonate deposits mix in the form of turbidity currents generating a deep-water fan system. In parallel, Francis et al. (2008) have presented an example of a mixed deep-water calciclastic-siliciclastic system in the Gulf of Papua, northeast Australia and southern Papua New Guinea. Here, mixed sediment derived from two different sources, resulted in the generation of channel-levee systems. More recently, Moscardelli et al. (2019) have documented a mixed siliciclastic-carbonate turbiditic depositional system offshore Nova Scotia (Back and Reuning, 2015; Dunlap et al., 2018).

This study aims to expand the current knowledge about deep- and ultra-deep water carbonate depositional systems (i.e. mixed calciclastic-siliciclastic systems) by using a case study from the Miocene to Holocene Pará-Maranhão (PAMA) Basin in Equatorial Brazil (Figs.

1 and 2). High-quality 3D seismic data are used to characterise the internal geometry of channel-levee systems formed in a mixed calciclastic-siliciclastic depositional system. Borehole data from the shelf margin document the thickness and composition variability of the so-called Ilha de Santana Platform and the PAMA continental shelf, which provide the main source of sediment to the continental slope and rise (Figs. 1 and 2). Hence, this work investigates the morphological expression of mixed calciclastic and siliciclastic sediment transfer from the PAMA shelf and the Ilha de Santana Platform, via the continental slope, on its way to deep and ultra-deep waters. Details about the Neogene stratigraphic succession of the PAMA Basin aim to provide a better understanding of new exploration plays in Equatorial Brazil. In summary, this paper intends to answer the following questions:

1. What types of depositional features characterise mixed calciclastic-siliciclastic systems in deep and ultra-deep-water environments?
2. Can deep-water channel-levee systems be formed on a carbonate-dominated continental margin recording minor siliciclastic input?
3. How similar are the geomorphic properties of channel-levee systems formed on carbonate-rich margins when compared to their siliciclastic counterparts?

As described in Playton et al. (2010), it is useful and important to understand the relationship between platform and basinal settings. This is because in many cases, platform-derived information is more robust than basin-related data. Our study area is such a case, as the continental slope and rise are imaged in seismic data, while exploration wells were, thus far, only drilled on the shelf margin (Fig. 1b).

2 Geological framework

The offshore Para-Maranhão (PAMA) Basin is located on the Brazilian Equatorial Margin and consists exclusively of marine deposits covering an area of about 48,000 km² (Soares et al., 2007) (Fig. 1). The basin is oriented NW-SE due to the effect of transtensional tectonics in its early development, being bounded by the Foz do Amazonas Basin to the northwest and the Barreirinhas Basin to the southeast (Zalán, 2015) (Fig. 1).

Hydrocarbon exploration started in the PAMA Basin during the 1970s and 1980s, via the acquisition of a series of 2D seismic profiles and the drilling of multiple exploratory wells. Most wells were deemed dry until the year of 1993, with the discovery of a sub-commercial oil show in fractured Cenozoic carbonates in the well 1-PAS-11 (Soares et al., 2007; Zalán, 2015). Interest in the region has increased in the past decade due to the economic potential of deep and ultra-deep water basins of Equatorial Brazil, which was enhanced by the discovery of large oil fields on the conjugate margins of Ghana and Ivory Coast (Henry et al., 2011). In fact, deep-water basins in West Africa and Equatorial Brazil have similar structural and sedimentary features (Henry et al., 2011; Zalán, 2015; Almeida et al., 2018, 2020; Da Silva and Ribeiro, 2018). In parallel, recent data in Zalán (2015) and Da Silva and Ribeiro (2018) describe a broad gravitational system in the PAMA and Barreirinhas basins, relating this same system to the deposition of overlying turbidites (e.g. GB1-4500, Figs. 1a, b and 3a).

2.1 Tectono-stratigraphic setting

The sedimentary history of the PAMA Basin is complex and started with the deposition of Paleozoic deposits over Precambrian intracratonic sequences (Soares et al., 2007; Zalán, 2015). This basin has been controlled since the Cretaceous by two major oceanic fracture zones, the Romanche and St. Paul; which are still active today (Nemčok et al., 2013). An

updated and detailed tectono-stratigraphic chart was published by Soares et al. (2007) in which the PAMA Basin is sub-divided into three supersequences: Pre-Rift (intracratonic), Rift, and Drift (Fig. 3a). Basal Paleozoic deposits from the intracratonic Pre-Rift Supersequence are inferred as similar to those in the Parnaíba Basin (Zalán, 2015). The latter basin comprises Paleozoic strata deposited over the São Luís Craton due to the fragmentation and breakup of northwestern Gondwana (Soares et al., 2007; Oliveira et al., 2012).

The Rift Supersequence was deposited under a transtensional tectonic regime and is divided into Aptian and Albian syn-rift (Rift II) and intra-rift (Rift III) deposits (Soares et al., 2007). Syn-rift strata are composed of continental sandstones and shales showing strata pinches in seismic sections. In between the two rift phases (Rift II and Rift III), a sag basin was developed and was filled by the Codó Formation, a unit of lagunar organic-rich shales, anhydrites and calcilutites (Soares et al., 2007). Their seismic response is characterised by parallel reflectors with good continuity. The Albian Rift III sequence is formed by siliciclastic deposits typical of delta fans accumulated in a marine environment (Brandão and Feijó, 1994; Soares et al., 2007). Comparisons with the Ceará Basin (Almeida et al., 2018, 2020) indicate this latter Rift III sequence to be a Breakup Sequence *sensu* Soares et al. (2012) and Alves and Cunha (2018).

The Late Albian to Recent Drift Supersequence comprises the Humberto de Campos Group, and is divided into three units: Areinhas (sandstones), Ilha de Santana (wide carbonate shelf), and Travosas formations (slope and turbidite deposits) (Soares et al., 2007; Zalán, 2015) (Fig. 3c). In addition, the study area contains gravitational systems in the Drift Supersequence that impose a marked structural zonation in the basin from its proximal to distal parts (Fig. 3a, b). As a result; extensional, transitional and contractional zones are identified from the shelf to the abyssal parts of the PAMA Basin (Zalán, 2001; Oliveira et al., 2012; Almeida et al., 2018) (Fig. 3a, b).

2.2 Regional stratigraphy

Brandão & Feijó (1994) first described the stratigraphic succession of the PAMA Basin based on data from 29 exploration wells and 45,500 km of 2D seismic profiles, sub-dividing the region into three groups: Canárias, Caju and Humberto de Campos (Fig. 3c). The Canárias Group consists of sandstones, siltstones and shales deposited by deltaic fans in a marine environment during the Early and Mid- Albian (Brandão and Feijó, 1994). The Caju Group consists of quartzose sandstone, shales and local bioclastic calcarenites accumulated in a neritic environment during the late Albian (Brandão and Feijó, 1994). The Humberto de Campos Group comprises Cenomanian to Recent deposits representative of a divergent margin, and includes the Areinhas, Ilha de Santana and Travosas formations (Figs. 3c and 4). The Humberto de Campos Group extends to the Barreirinhas Basin and its youngest strata are the focus of this work.

The Areinhas Formation is composed of quartzose sandstone packages intercalated with shales, siltstone and calcilutite. The Ilha de Santana Formation comprises a thick carbonate succession with the presence of calcarenites and calcilutites intercalated with shales and marls. Turbidites are common on the continental slope. The Travosas Formation is a typical coastal-platform-slope system and, at its most distal part, is known to comprise deposits of shales and siltstones intercalated with quartzose sandstones (Brandão and Feijó, 1994; De Souza, 2006; Piovesan, 2008). However, based on the well data later described in Section 5, parts of the Travosas Formation are also dominated by calciclastic deposits. In essence, a mixed calciclastic-siliciclastic system sourced by the Ilha de Santana Platform fed the continental slope and rise as a result of slope instability, turbidity and marine currents.

2.3 Carbonate-platform development off PAMA

In the latest Cretaceous-earliest Paleogene, the main sediment input to the PAMA Basin was siliciclastic, and the Ilha de Santana Platform was still an emerged area (Soares Júnior et al., 2011). According to Soares et al. (2007), a sea-level lowstand dominated the evolution of the PAMA Basin during the upper Eocene and lower Oligocene, narrowing the carbonate shelf and exposing it to subaerial conditions. This facilitated the development of dolomitic intervals in the Ilha de Santana Formation (Soares et al., 2007).

During the late Oligocene-middle Miocene, the Equatorial Margin of Brazil was dominated by the development of a large carbonate platform in a shallow-water palaeoenvironment (Soares et al., 2007; Soares Júnior et al., 2011; Rossetti et al., 2013; Aguilera et al., 2020). This carbonate platform extended from the Foz do Amazonas Basin (Figueiredo et al., 2007; Aguilera et al., 2020), to the PAMA (Soares et al., 2007), Barreirinhas (Trosdorf Junior et al., 2007) and the Ceará basins (Soares Júnior et al., 2011). In the Foz do Amazonas Basin, carbonate productivity terminated around the late Miocene-Pliocene as a consequence of Andean tectonics, which led to a rearrangement of the palaeo-Amazon River and the subsequent onset of clastic sediment input from both the Amazon delta and coastal plain drainage systems (Figueiredo et al., 2007; Soares Júnior et al., 2011; Aguilera et al., 2020). In the three other basins mentioned above, carbonate productivity continued until the present-day, as recorded in well data crossing the Ilha de Santana Formation (Fig. 5) and published stratigraphic data from the Ceará and Barreirinhas basins (Soares Júnior et al., 2011; Aguilera et al., 2020). In the PAMA Basin, Aguilera et al. (2020) identified minor siliciclastic input near the shore during the Miocene, sourced from small river mouths such as the Gurupí River (Fig. 1b).

3 Datasets and methods

3.1 Seismic data

This study uses a full-stack depth-converted 3D seismic volume (3D PAMA PSDM Full Stack) covering an area of about 1,950 km² in the PAMA Basin, Equatorial Brazil (Figs. 1a, b and 2). Our dataset images the edge of the continental shelf, together with the continental slope and continental rise, in water depths ranging from 100 m to 3,500 m (Figs. 2 and 3b). The seismic volume, provided by Polarcus, consists of 3201 inlines (IL) and 3901 crosslines (XL) with a 12.5 x 12.5 m line spacing and a sampling interval of 5 m. The interpreted seismic data were processed in the depth domain with a SEG positive polarity using the European convention; an increase in impedance is represented by a red (positive) peak (Fig. 3b). The high-quality seismic data allow for the detailed analysis of stratigraphic and seismic facies to a depth of 7,500 m below the sea floor (Fig. 3b). In this study, we focus on the Miocene to Holocene stratigraphic successions of the PAMA Basin (Figs. 3b, c and 4).

In addition to 3D seismic data, we use public 2D seismic sections to complement our study. The regional 2D seismic profile GB1-4500 was reinterpreted from Henry et al. (2011) and Zalán (2015) as to provide information on the PAMA Basin at the scale of the continental margin (Figs. 1b and 3a). Regional 2D seismic profile 022-0837 (Fabianovicz, 2013), and seismic profiles 0270-3010 and 0275-8780 (Da Silva and Ribeiro, 2018), were used to correlate the seismic stratigraphy of our study area with main depositional sequences recognised on borehole and outcrop data (Fig. 1b).

3.2 Well data

Well data are scarce in the PAMA Basin, with only a few exploration wells spudded in shallow waters of the carbonate shelf margin. No wells have been drilled on the continental

slope and rise within the interpreted seismic survey. Composite data from seven (7) exploration wells were provided by the Brazilian National Agency of Petroleum, Natural Gas and Biofuels (ANP) (Fig. 5). The exploration wells are located near the edge of the continental shelf and document the shallow-water depositional systems transporting sediment into deep waters (Fig. 5). Well data include gamma-ray, deep-resistivity and lithological logs (Fig. 5).

3.3 Seismic interpretation and channel definition

Our seismic-stratigraphic interpretation is based on published literature from Fabianovicz (2013), Da Silva and Ribeiro (2018), and Alves et al. (2020). Stratigraphic data for the basin derive from the work of Brandão & Feijó (1994), Soares et al. (2007) and university theses such as De Souza (2006), Da Silva (2007) and Piovesan (2008). A summary of the methodology used to analyse the depositional systems and geomorphic parameters of channel-levee systems is shown in Fig. 6.

The offshore PAMA Basin is still an exploration frontier with limited data available in existing publications. However, a few published 2D seismic profiles intersecting our 3D survey were useful to gain a regional understanding of the basin (Fig. 1b). In this study, we reinterpreted a portion of the GB1-4500 seismic profile to provide a regional context for the PAMA Basin (Fig. 3a). This pre-stack depth migrated (PSDM) 2D seismic profile GB1-4500 from ION's Greater Brazil SPAN project has been previously interpreted by Henry et al (2011) and Zalán (2015). Published interpretations of 2D seismic profiles 0222-0837 from Fabianovicz (2013), and 0270-3010 and 0275-0780 from Da Silva et al. (2018), provided us with additional stratigraphic information (Fig. 1b). A portion of the seismic profile 0275-8780 is shown in Fig. 5c and 5d together with a projection of well 1-MAS-16.

Seismic interpretation was completed using Schlumberger's Petrel® and based on the general principles of seismic stratigraphy; hence, we interpreted reflection terminations, seismic facies and seismic units in great detail (Cross and Lessenger, 1988; Catuneanu, 2006). In total, five key seismic horizons (H₁ to H₅) were interpreted, together with the seafloor (SF), in Miocene to Recent strata (Figs. 3b, 4 and 7). Two regional unconformities (Top Oligocene and Top Cretaceous) were also interpreted and considered to be key stratigraphic markers in the study area (Figs. 3b and 4). Channel-levee systems were mapped on specific seismic horizons (Figs. 6, 7 and 8).

Seismic interpretation near the continental slope and also within channel systems is difficult due to their complex geometries and poor continuity of seismic reflections (Fig.8). To tackle this problem, seismic attributes such as instantaneous phase and cosine of phase are computed and displayed with a certain degree of transparency over the amplitude volume, so as to better identify the continuity of particular seismic reflectors (Fig. 6). A surface grid with a cell size of 25x25 m is used to generate structural maps (Figs. 6 and 7). Based on a previously calculated variance attribute volume, the variance attribute is extracted with a search window of 20 m for every depth map (H₁ to H₅, and SF) (Fig. 6). This latter seismic attribute is crucial in our analysis as it highlights discontinuities in each seismic horizon, improving the imaging of stratigraphic features and facilitating channel recognition (Fig. 7).

Both depth and extracted variance raster maps have been imported into ArcGIS to digitise and delineate discrete channel-levee systems (Fig. 6). For an enhanced visualization, depth maps are overlaid by variance maps with a 50% transparency (Fig. 7). A 3D visualisation of key maps is also useful to better recognise channel-levee systems and other sediment conduits (Fig. 7).

3.4 Geomorphic parameters

A similar methodology to Gee et al. (2007) and Lemay et al. (2020) is adopted in this work to analyse the morphometric parameters of channel-levee systems in the PAMA Basin (Fig. 6). Lemay et al (2020) introduce a quantitative geomorphic classification and methodology to analyse submarine sediment conduits based on cross-sectional and planform data. Their classification helps to differentiate between sediment conduits with and without the presence of levees. In parallel, Gee et al. (2007) examines and quantifies key geometric parameters in deep-water submarine channels to better understand the main controls on submarine channel geometry, as well as on their initiation and evolution. The latter authors focus on siliciclastic systems, and this work aims to compare and differentiate their models to the calciclastic systems of the PAMA Basin.

Cross-sectional parameters are measured every 3 to 5 km along the channel thalwegs, in perpendicular profiles to these latter. Measurements include width (W), mean depth ($L_{h_{\text{mean}}}$), maximum depth ($L_{h_{\text{max}}}$) and area; parameters used later in this work to classify the interpreted channels (Fig.8). The upper limits of asymmetric levees are precisely defined for each channel. In our measurements, the mean depth ($L_{h_{\text{mean}}}$) is the ratio of the cross-sectional area to the bankfull width of a channel (Figs. 8 and 9).

Parameters used in this work to characterise channel planform geometries include sinuosity, meander amplitude (A) and meander wavelength (λ) and are measured using a Python Jupyter Notebook provided by Lemay et al. (2020). This algorithm is based on Sylverster and Pirmez (2017) script, allowing for consistent measurements of all studied channels. The processing steps of the Lemay et al. (2020) algorithm are as follows: (1) x and y coordinates of the channel centrelines are resampled with a 50 m spacing; (2) centrelines are smoothed out for a given window length using the Savitzky-Golay filter (Savitzky and Golay, 1964). (3) The curvatures of the centreline are computed to determine inflection points in

channels; (4) the number of channel bends are defined by computing inflection and apex points; and (5) geometric parameters (sinuosity, λ and A) are computed for each channel bend. In this work, conduit bed slope is measured every 3 to 5 km based on the thalweg depth obtained from seismic profiles. A value of about twice the mean channel width is used in Step 2 above, to scale the window length to the interpreted channels.

3.5 Statistical analysis

The morphometric parameters of the PAMA calciclastic channel-levee systems are plotted on box- and cross-plots (Figs. 10 and 11). Box plots show the statistical distribution of the morphometric parameters for each channel-levee system (Fig. 10). Cross-plots show the relationships between specific morphometric parameters (i.e. mean bankfull depth, bankfull width, meander amplitude and meander wavelength) (Fig. 11). Least-square linear regressions were computed on log-transformed data for all calciclastic channel-levee systems together, as to obtain a power-law equation (Fig. 11). A regression curve with its associated 95% confidence interval is shown only when the coefficient of determination R^2 is higher than 0.1 to avoid non-correlation hypotheses (Fig. 11).

Calciclastic morphometric relationships are compared to established models (i.e. power-law equations) of siliciclastic submarine conduits from Lemay et al. (2020) and fluvial channels from Williams (1986) and Held (2011) (Fig. 11). Data from Lemay et al. (2020) are plotted to document the differences between siliciclastic submarine conduits and calciclastic channels (Fig. 11).

4 Physiography and sedimentary environment

The modern PAMA continental shelf is 150 km to 250 km wide. Water depth along the shelf-slope profile transitions from shallow waters with an average depth of 25 m on the continental shelf to 3,500 m in ultra-deep waters (Figs.1, 2 and 3). The PAMA continental shelf is a tectonically steepened carbonate ramp with no rimmed reef along its margin (Alves et al., 2020). The study area has been considered as a mixed carbonate-siliciclastic shelf in all similar to the analogous Ceará Basin (de Morais et al., 2019) (Fig.1a).

Recent data from Ceará identified three main depositional systems on its continental shelf: a) siliciclastic, located near the shoreface and river mouths, b) mixed, comprising biolithoclastic and lithobioclastic facies and, c) carbonate, revealing the predominance of an autochthonous carbonate supply, mainly derived from calcareous algae (de Morais et al., 2019). The modern carbonate shelf of Equatorial Brazil is itself considered to be a major supplier of carbonate deposits to more distal regions as its middle and outer parts record typical autochthonous carbonate sedimentation (de Morais et al., 2019). The inner continental shelf is characterised by the mixing of siliciclastic and carbonate sediment, especially during maximum freshwater discharges from suspended sediment released from river mouths (de Morais et al., 2019). An exception to this setting is the Foz do Amazonas Basin, which is dominated at present by the large siliciclastic input from the Amazon River and Delta, feeding sediment into deep waters via a large submarine channel (Fig. 1a).

Siliciclastic input from rivers such as Gurupí and Turiaçu in PAMA can be compared to the depositional setting observed in Ceará, as they have similar settings (Fig. 1c). In Ceará, the transporting distance of suspended sediment sourced from near the shoreline have been studied around the Parnaíba and Jaguaribe rivers, where siliciclastic material is transported up to 10 km oceanward from the river mouths (Dias et al., 2013; Aquino da Silva et al., 2015) (Fig. 1a). In order to verify how far siliciclastic sediment can travel on the modern PAMA shelf today,

we used a comparable approach to Aquino da Silva et al. (2015) and Morais et al. (2019) (Fig. 1c). In this work, we utilised a combination of multispectral satellite imagery with bands B4-Red, B3-Green, and B1-Ultra blue (coastal aerosol) provided by the Sentinel-2 mission (Fig. 1c). Sediment suspended in water can be traced by using the coastal aerosol band (B1), as this band reflects the blue and violet colour spectra displaying subtle differences in the colour of water (Hedley et al., 2018). The interpreted multispectral satellite data prove that sediment from rivers in PAMA is transported 20 km to 50 km off the shoreline (Fig. 1c). This pattern is similar to that observed on the Ceará continental shelf (de Morais et al., 2019, Fig. 1), suggesting that the inner shelf in PAMA is also dominated by the deposition of siliciclastic sediment (Fig. 1c).

Well data from PAMA document the presence of calcarenite and calcilutite deposits on the outer continental shelf (Fig. 5). In PAMA, there are no scuba diving or sedimentary cores such as the ones analysed in Ceará by de Morais et al. (2019), but the well data shown in this paper still reveals similar depositional systems to those recognised in Ceará. On both the PAMA and Ceará basins, the middle and outer continental shelf reveal the predominance of autochthonous carbonate sediment (de Morais et al., 2019).

Based on the observations above, we can suggest that beyond the inner 50 km zone of the PAMA continental shelf, dominated by episodic siliciclastic input, there is a healthy development of a carbonate depositional system such as the one observed off Ceará. In our study area, this carbonate system extends up to 150 km to 165 km away from the inner zone, and occurs on the herein called middle and outer continental shelf (Fig. 1c). Beyond the shelf edge, submarine canyons develop on the continental slope and transition to channel-levee systems in ultra-deep waters (Fig. 2). The outer continental shelf, dominated by carbonate deposition with calcarenites and calcilutites, is the primary sediment source feeding the channel-levee systems recognised beyond the shelf edge. Deep-water depositional systems in

PAMA can be considered as pure carbonate systems given the presence of a wide area of carbonate deposition on the Ilha de Santana Platform. However, because of the presence of siliciclastic deposits on the inner continental shelf, it is more conservative to consider these same deep-water depositional systems as mixed calciclastic-siliciclastic. This is because siliciclastic input can be transported away from the inner shelf to the proximity of the shelf break and upper continental slope due to marine currents acting on the shelf, such as the documented in the Gulf of Papua and North Queensland, Australia (Francis et al., 2008). Additional data such as piston core samples would be useful to confirm this interpretation.

5 Borehole stratigraphic interpretation

Seven (7) exploration wells provide important stratigraphic data in the study area and complement the stratigraphic column in Soares et al. (2007) (Figs. 4 and 5). Well 1-MAS-9 drilled 1658 m of strata in the Ilha de Santana Formation comprising thick successions of calcarenites with intercalated packages of calcilutites (Fig. 5). Below this latter unit, Well 1-MAS-9 crossed a thin package of the Travosas Formation consisting of carbonate deposits (calcarenites and calcilutites) intercalated with sandstone intervals up to 3 m-thick (Fig. 5). This is an important observation because it shows carbonate deposition to predominate on the continental slope of PAMA, a character contrasting with previous interpretations of the Travosas Formation as a siliciclastic-dominated unit (e.g. Brandão and Feijó, 1994; De Souza, 2006; Piovesan, 2008).

Well 1-MAS-16 found 3450 m of Paleogene-Neogene strata in the Ilha de Santana Formation consisting of thick packages of calcarenites intercalated with thin layers of calcilutites and calcisiltites with sparse layers of marls and dolomite (Fig.5). Towards the base of the formation there are more frequent, and thicker calcisiltite intervals. Well 1-MAS-16 is

the only well with available chronostratigraphic data, although only for Cretaceous strata (Piovesan, 2008). Here, the Travosas Formation shows a greater presence of siliciclastic material, mainly intervals of shale and marl intercalated with calcisiltite layers (Fig. 5). Well 1-MAS-16 is also important as it can be projected and tied to seismic profile 0275-8780 from Da Silva and Ribeiro (2018) (Fig. 5c, d). Paleocene-Oligocene strata appear to be dominated by the development of a thick carbonate shelf. Miocene to Recent strata reveal the aggradation of a growing, healthy carbonate shelf (Fig. 5c, d).

Well 1-MAS-19 found 3193 m of strata in the Ilha de Santana Formation, which comprises calcarenites in its upper part (Fig. 5). Below a depth of 2140 m, the Ilha de Santana Formation reveals significant siliciclastic input in the form of 5 m- to 10 m- thick layers of sandstones and marls (Fig. 5). Well 1-MAS-19 also drilled through 603 m of intercalated sandstones, siltstones and shales in the Travosas Formation (Fig. 5).

Wells 1-MAS-24 and 1-MAS-10 respectively drilled 4108 m and 3946 m of the Ilha de Santana Formation in the thickest part of the continental shelf (Fig. 5). In contrast, wells 1-MAS-25 and 1-MAS-27A drilled the thinnest portion of the carbonate shelf, recording 1252 m and 1630 m of intercalated calcarenite and calcilutite packages (Fig. 5). Thin layers of sandstone and shale are observed in these two wells, suggesting episodic pulses of siliciclastic material transported from the inner continental shelf to its outer part. Wells 1-MAS-25 and 1-MAS-27A also reveal the presence of a 97 m and 110 m thick Areinhas Formation, chiefly consisting of sandstone and shale (Fig. 5).

Well 1-MAS-25 found 183 m of the Travosas Formation with intercalations of sandstone, shales and calcarenites (Fig. 5). The Travosas Formation in wells 1-MAS-9 and 1-MAS-25 documents that, during the Maastrichtian, there was a mixed carbonate-siliciclastic depositional system on the upper continental slope of the PAMA Basin. In addition, the seven

wells interpreted in this work confirm the presence of a thick Cenozoic carbonate shelf in the study area, with thin siliciclastic deposits. This suggests that distal slope deposits in the Miocene to Recent PAMA Basin are mainly dominated by redeposited calciclastic sediments with occasional compositional mixing with siliciclastic deposits (Fig. 5).

6 Seismic-stratigraphic framework of PAMA

Four Miocene-Holocene seismic units were interpreted in the PAMA Basin and named, from the oldest to the youngest, as Units 1 to 4 (Figs. 3b and 4). These stratigraphic units lie on top of the gravitational complex imaged in Fig. 3b. The Top Cretaceous (TK) horizon was mapped first to provide a key reference to our structural analysis (Fig. 3b, c). The Top Oligocene (TO) horizon marks a major regional unconformity in the PAMA Basin caused by a global sea-level fall (Gradstein et al., 2005; Soares et al., 2007) (Fig. 3b). Faults related to the slope gravitational complex terminate at horizon TO (Fig. 3b). In the study area, the unconformity forms a high amplitude reflector with onlapping strata above it (Fig. 3b), as also recognised in the Barreirinhas and Foz do Amazonas Basins (Soares et al., 2007; Da Silva and Ribeiro, 2018). Above the TO unconformity, a general aggradational setting for the PAMA carbonate shelf has been previously suggested by Soares et al. (2007).

Multiple channel-levee systems occur close to or on Miocene to Recent horizons H₁ to H₅ (Fig. 7). These systems occur in Seismic Units 1 to 4 described below. Based on descriptions in Soares et al. (2007) and Rosetti et al. (2013), we have correlated our seismic units to the sequences defined in Soares et al. (2007) (Fig. 4).

6.1 Unit 1 - Lower Miocene

Unit 1 is characterised by its high to medium sub-parallel internal reflections. It is bounded at its base by the TO horizon and onlaps this latter unconformity to the southwest (Fig. 3b). Horizon H₁ marks the top of Unit 1 and comprises a high amplitude, sub-parallel seismic reflector (Fig. 7k, l).

Unit 1 is correlated with Sequence E80-N10 in Soares et al (2007), recognised as a major Cenozoic transgressive event (Fig.3). This event is associated with the maximum expansion of carbonate deposition on the PAMA continental shelf. On the continental slope, horizon H₁ is characterised by the incision of a small and sinuous channel and the formation of a calciclastic submarine fan as shown in Figs. 7k and 7l.

6.2 Unit 2 - Middle Miocene

Middle Miocene strata in Unit 2 is bounded by horizons H₁ and H₃, and onlaps the Top Oligocene unconformity to the southwest (Figs. 3b and 4). This unit has medium- to high-amplitude reflections, and is correlated with Sequence N20-N30 defined in Soares et al. (2007). Horizon H₂ is observed half-way through Unit 2 as a low- to high- amplitude discontinuous reflection. The formation of a large channel (channel *c*) is first observed at the level of horizon H₂ (Fig. 7i, j).

The top of Unit 2 coincides with horizon H₃, a moderate-amplitude reflector (Fig. 4). This unconformity has been considered as an important feature on Brazil's Equatorial Margin in seismic and well data (Soares et al., 2007). Although its amplitude is not as high as the Top Oligocene (TO) unconformity, horizon H₃ marks a relative sea-level drop across the PAMA Basin (Figs. 3b and 7g, h).

6.3 Unit 3 - Upper Miocene-Pliocene

Unit 3 correlates with Sequence N40-N50 in Soares et al. (2007) (Fig. 4). The unit is bounded at its base by horizon H₃ and at its top by horizon H₅ (Fig. 4). Strata in this unit mark a phase of progradation of the PAMA continental shelf (Soares et al., 2007). A low- to medium-amplitude, sub-parallel reflector (Horizon H₄) separates Upper Miocene and Pliocene strata within Unit 3 (Figs. 3b and 4). Horizon H₄ is incised by Holocene channels and canyons on the continental slope.

6.4 Unit 4 Pleistocene to Recent

Pleistocene to recent strata lie above horizon H₅, a medium-amplitude continuous reflector. The seafloor (SF) bounds Unit 4 at its top. This unit has low-amplitude continuous reflections and correlates with Sequence N60 in Soares et al. (2007) (Fig. 4).

7 Morphology of calciclastic submarine fans and levee-channels

7.1 Calciclastic submarine fan a

Linear features are recognised in horizons H₁, H₂, and H₃, and are interpreted as erosional distributary furrows (Fig. 7k, l). These furrows suggest the presence of a turbidite system with a sediment flow direction towards the north, which created a large submarine fan. Sediment flow is funnelled by conduit *a*, widely opening from the continental slope onto the continental rise.

Channel-levee systems started to develop within the calciclastic submarine fan at the level of horizon H₃ as a result of the continuing incision of the erosional furrows (Fig. 7g, h). Channel *a* became, at this time, the major feature at this level (Fig. 7g, h). In Horizons H₄ and

H₅, the submarine fan becomes narrower, but with channel *a* still growing in size (Fig. 7c-f). The Holocene submarine fan is no longer observed on the modern sea floor, but channel *a* has grown considerably when compared with its Miocene and Pliocene counterparts (Fig. 7a, b). At present, conduit *a* forms a deep, incised canyon at the shelf margin, spanning to the continental rise, where it becomes a channel-levee system (Fig. 7a, b). Channel *a* is the main feature on the modern sea floor with a minimum length of 56 km, continuing to the north beyond the limits of the seismic data (Figs. 2 and 7a, b).

Morphometric data for channel *a* increase consistently as the channel evolved from horizons H₄ to the seafloor (Fig. 10). Cross-sectional area and bankfull width suggest that channel *a* developed over time (Fig. 10e, f). Similarly, conduit bed slope and sinuosity also increase from H₄ to the sea floor. Mean slope varies from 1.6 at H₄, to 2.5 at horizon H₄, and reaches a value of 3 on the sea floor, a character that proves continuing channel incision (Fig. 10a). Sinuosity, however, shows that as the channel evolved, its amplitude and wavelength increased, reaching values of 1.04 to 1.09 (Fig. 10b-d).

7.2 Channel b

Channel *b* is first recognised in horizon H₄, developing on the continental slope (Fig. 7e, f). Similarly to channel *a*, this sediment conduit grew from horizon H₄ to the sea floor (Fig. 7). An aggradational stacking pattern is recognised in cross-section, suggesting a continuous sediment input to channel *b* through time (Fig. 8). Area and bankfull width of the channel increase upwards (Fig. 10e, f). Conduit bed slope and sinuosity do not markedly change, recording mean values of 5.0-6.0 and 1.08-1.12 %, respectively (Fig. 10a, b).

7.3 Channel c

Channel *c* shows flanking levees, a character similar to the previous two channels (Figs. 8 and 9). Planform and cross-sectional parameters of channel *c* are comparable to channels *a* and *b*; they are all aggradational, with area, bankfull width and bed slope increasing as the channel evolved (Figs. 7, 8, 10). The difference between channel *a* and *c* is that channel *c* starts as a discrete channel-levee system at the level of horizon H₂ and no submarine fan is observed (Fig. 7k, l). Cross-sectional area increased from 21217.3 m² in horizon H₂ to 276135.7 m² on the sea floor. Mean bankfull width values also increase from 756.7 m at horizon H₂ to 2098.1 m on the sea floor. Mean bed slope rises from 1.5% at H₂ to 4.7% on the seafloor. Sinuosity values are similar at different stratigraphic levels, with low mean values ranging from 1.09 to 1.18 (Fig. 10b).

7.4 Channels d, e and f

Channels *d*, *e* and *f* are first observed on the continental slope at the level of horizon H₃ (Fig. 7g, h). The seismic data in this work only image the development of these conduits as canyons on the continental slope, and they appear to merge into one channel near the limit between the continental slope and continental rise. The funnelled channels *d*, *e* and *f* extend beyond the limits of our seismic data (Fig. 7 g, h).

7.5 Channel x

Channel *x* is only identified in horizon H₂ (Figs. 7c, d and 8). Cross-sectional data show that channel *x* did not evolve beyond horizon H₂ (Fig. 8). Its mean cross-sectional area is 29111.0 m² and its mean bankfull width is 1019.1 m. Conduit bed slope is 2.5% on average and mean sinuosity is low, reaching a value of 1.1 (Fig.10).

553

554 **7.6 Channel y**

555 Channel y is only observed in horizon H₁, showing a sinuous morphology that contrasts
556 with the previous channels (Fig. 7k, l). In cross-section, channel y is a small channel that
557 aggrades a few reflections above horizon H₁, dying out below horizon H₂ with characteristic
558 low amplitude, parallel internal reflections (Figs. 8 and 9). Mean cross-sectional area and mean
559 bankfull width are the smallest recognised when compared to the other channels, with values
560 of 6169.8 m² and 417.6 m, respectively. Its mean conduit bed slope is 2.18% with a high mean
561 sinuosity of 1.39 (Fig.10).

562

563 **8 Channel morphometric relationships**

564 Channel morphometric data are here compared to power-law regressions concerning
565 submarine and fluvial channels formed in siliciclastic environments (Williams, 1986; Held,
566 2011; Lemay et al., 2020). These results confirm that calciclastic channels in the PAMA Basin
567 have a degree of similarity to their siliciclastic counterparts.

568 Width vs. depth relationships for the interpreted calciclastic channel-levee systems are
569 comparable to the siliciclastic channel models proposed by Lemay et al. (2020), in which
570 channel sizes are similar (Fig. 11 a, b). However, differences in the exponents and coefficients
571 of the power-law distribution display a less steep curve for calciclastic channels (Fig. 11a, b).
572 The latter have larger levee heights than siliciclastic channels for a given bankfull width (Fig.
573 11 a, b). Wavelength and amplitude regression data also show a less steep curve (Fig. 11c, d).
574 Thus, calciclastic channels are slightly more sinuous than siliciclastic channels, as their
575 amplitude is higher for a given wavelength (Fig. 11c, d). Data from channel y are particularly
576 interesting as they plot closer to the model of fluvial channels of Williams (1986), thus

justifying why channel *y* shows higher sinuosity values than the other calciclastic channels (*a*, *b*, *c* and *x*) (Fig. 11c, d). Abandoned channels are also observed from seismic data around channel *y*, revealing another similarity with meandering fluvial channels (Fig. 6e, f).

Bankfull width vs. meander amplitude and bankfull width vs. meander wavelength relationships for calciclastic channels have low correlation values of the power-law distribution, ranging from 0.04 to 0.22 (Fig. 11e-h). When compared calciclastic channel data to siliciclastic channel data from Lemay et al. (2020), it is evident that this type of relationship display a lower correlation (Fig. 11e-h).

9 Discussion

Oil and gas exploration on continental margins has advanced our knowledge of deep-water depositional systems, as the latter contain large hydrocarbon fields (Weimer and Slatt, 2004; Kang et al., 2018; Lemay et al., 2020). Examples of deep-water basins with hydrocarbons include the Campos Basin in Brazil, the Gulf of Mexico, the Niger Delta Basin and the Congo Fan Basin in West Africa; basins that account for 70% of the global deep-water reserves to date (Kang et al., 2018). Furthermore, it is important to address the evolution and depositional character of deep-water systems in any offshore activity. Gravity flows in deep-water channels can impact to deep-water infrastructure such as submarine cables, pipelines, or the foundations of offshore wind farms (Schneider and Senders, 2010; Baker et al., 2016; Clare et al., 2017).

Calciclastic systems are important to understand sediment transfer off carbonate shelves and isolated carbonate platforms. In the case of isolated carbonate platforms, it is relatively easy to recognise pure carbonate systems in deep waters as they comprise, locally, the only source of carbonate sediment. An example of this is the Glorieuses archipelago in the SW Indian Ocean, in which around an isolated carbonate platform, channel-levee complexes and

turbiditic lobes were developed at water depths of 2000-3400 m (Jorry et al., 2020). In contrast, carbonate shelves have a more complex setting as they often occur adjacently to siliciclastic depositional systems. A well-documented example is the Gulf of Papua between NE Australia and S Papua New Guinea, where siliciclastic material sourced from rivers draining the Papuan Peninsula mix with carbonate deposits from the shelf and isolated carbonate platforms (Francis et al., 2008).

9.1 Mixed calciclastic-siliciclastic depositional systems in the deep and ultra-deep PAMA Basin

This work stresses the presence of a mixed calciclastic-siliciclastic depositional system on the distal continental slope in PAMA during the Miocene to Holocene, as revealed by the Travosas Formation. So far, there are no wells drilled on the distal continental slope and ultra-deep waters of PAMA to confirm the latter assumption, but based on well data from the shelf margin, we suggest a similar stratigraphy to the one observed in wells 1-MAS-9 and 1-MAS-16. In these wells, the Travosas Formation is dominated by carbonate deposits intercalated with minor siliciclastic intervals (Fig. 5). Throughout the Miocene to Holocene, the PAMA continental shelf has developed a similar environment to what we see today as reported in Soares Júnior (2002) and Soares Júnior et al. (2011). During the Miocene, the Ilha de Santana Platform was submerged forming a wide area with carbonate sediment ready to be redeposited in deep waters (Figs. 14-17 in Soares Júnior et al. 2011). Similarly, the Tiracambu mountain has sourced the inner PAMA continental shelf with siliciclastic material since the Miocene to Recent via small rivers (Fig. 1a).

The development of deep-water depositional systems is controlled by multiple factors such as basin tectonics, sea-level fluctuations, and the rates, types and sources of sediment

supply (Payros and Pujalte, 2008). According to Payros and Pujalte (2008) the most important factor generating a calciclastic submarine fan is the existence of an efficient funnelling mechanism forcing sediment gravity flows to merge downslope. Despite an initial line-source of sediment gravity flows, the physiographic profile of distally steepened ramp slopes allows the conversion of gullies and canyons to build up a point-sourced sedimentary accumulation. In our study area we can observe from horizons H_1 to the sea floor that, for the calciclastic submarine fan *a*, there is a relatively line-source of canyons, which merge together on the continental slope to create a point-source and funnel sediment coming from the shelf margin (Fig. 7). Seafloor maps are the best way to understand this process, as the whole continental slope is better imaged (Figs. 2 and 7a, b). The modern slope shows a wide array of canyons along PAMA's margin and near the border to the continental rise, some canyons merge into a single sediment conduit (Figs. 2 and 7a, b).

The way sea level affects sediment transport is distinct when comparing siliciclastic to carbonate depositional systems (Kendall and Schlager, 1981; Ma et al., 2018; Jorry et al., 2020). It is generally known that siliciclastic sediments can dominate deep-water deposition during a falling-stage or lowstand in sea level, as the inner continental shelf is exposed sub-aerially and usually connected to point-sources of sediment such as rivers, which are thus able to supply sediment directly into deep-water depocentres (Kendall and Schlager, 1981; Ma et al., 2018; Jorry et al., 2020). Submarine canyons are also commonly formed in falling-stage and lowstand periods in sea level. In contrast, carbonate basins during sea-level lowstands record a decrease in carbonate productivity as the shelf is also sub-aerially exposed and fails to export carbonate sediment into deep waters (Droxler and Schlager, 1985; Glaser and Droxler, 1993; Andresen et al., 2003; Jorry et al., 2008; Ma et al., 2018).

During sea-level transgressions and highstands, the supply of siliciclastic sediment is reduced as river deltas retrograde and the shorelines retreat landward (Droxler and Schlager,

1985; Glaser and Droxler, 1993; Andresen et al., 2003; Jorjy et al., 2008; Ma et al., 2018). Sea-level highstands are stages in which organic productivity increases on carbonate shelves allowing for their lateral expansion. The accompanying increase in slope instability has demonstrated that this stage promotes the transport of calciclastic sediment into deep-water basins (Droxler and Schlager, 1985; Glaser and Droxler, 1993; Andresen et al., 2003; Jorjy et al., 2008; Ma et al., 2018). Ramp aprons, calciclastic submarine fans, channel-levee systems and elongate lobes of mud-rich calciturbidites are characteristic of transgressive and highstand periods in sea level (Droxler and Schlager, 1985; Glaser and Droxler, 1993; Andresen et al., 2003; Jorjy et al., 2008; Ma et al., 2018). As an example, Tournadour et al. (2017) explain that submarine canyons in the Bahamas are related to slope failure followed by different stages of regressive erosion on isolated carbonate platforms.

Recent studies have proven that sea-level lowstand periods contribute to exporting calciclastic material into deep-water basins. Jorjy et al. (2020) demonstrate that certain topographic features on the shelf break and leeward slopes play an important role on carbonate shelves by storing sediment that is initially shed during sea-level highstands to be later re-mobilised during lowstands as calciturbidite deposits. This suggests that some calciturbidites behave like siliciclastic turbidites. Examples include the channel-levee complexes of the Glorieuses archipelago, SW Indian Ocean (Jorjy et al., 2020), and calciturbidites in the Northern Nicaragua Rise (Reijmer and Andresen, 2007), the Exuma Sounds, Bahamas (Reijmer et al., 2012, 2015b), and deposited along the Great Barrier Reef (Puga-Bernabéu et al., 2014). Furthermore, Payros and Pujalte (2008) suggest that in carbonate ramps with no rimmed platforms, such as in PAMA, shallow-water sediment production is generally not interrupted in distally steepened ramps during lowstands because productive zones in shallow waters can shift basinwards (Wright and Burchette, 1998; Payros and Pujalte, 2008).

The data in this work reveal a complex scenario when considering the development of calciclastic submarine fans and channel-levee systems in the PAMA Basin during the Miocene to Holocene. The whole Equatorial Margin of Brazil experienced similar conditions, therefore it is common in the literature to correlate observations from adjacent basins (Soares et al., 2007; Piovesan, 2008; Rossetti et al., 2013). Sea-level curves for the PAMA Basin can be extrapolated from outcrop observations of the Pirabas and Barreiras formations (Rossetti et al., 2013) (Fig. 4). The study from Rossetti et al. (2013) concluded that two major marine transgressive episodes occurred in Equatorial Brazil, one in the Oligocene-Miocene and the other in the early-middle Miocene (Fig. 4). Both events correlate with sea-level highstands recorded in other South American basins and also worldwide (Rossetti et al., 2013). Oligocene-Miocene marine deposits are represented by the Pirabas Formation, which accumulated at a time when a rise in sea level was recorded in several parts of the world. Rossetti et al. (2013) also reported a sea-level drop immediately before the start of the late Miocene with no subsequent transgressions being recorded, at least until the late Quaternary. This drop in sea-level is recognised by the development of a regional unconformity and formation of a lateritic soil at the top of the Barreiras Formation.

During the late Oligocene-lower Miocene (Sequence E80-N10), there was a major transgressive event covering all the Brazilian Equatorial Margin, associated with the Pirabas Sea, leading to an expansion of the carbonate shelf (Soares et al., 2007). These observations coincide with the transgressive episode reported in Rossetti et al. (2013) (Fig. 4). Upper Oligocene-lower Miocene strata are considered part of Unit 1 in this work. At the top of Unit 1 (horizon H₁), a sinuous channel (channel y) is recognised as well as several linear furrows forming a calciclastic submarine fan funnelled by sediment conduit *a* (Fig. 7k, l). Furrows can be related to turbidity flows similar to those recorded in the Little Bahama Bank (Tournadour et al., 2017), and cover a large area with no developed channels at this time (Fig. 7k, l). This

interpretation agree with the model proposed by Payros and Pujalte (2008) in which the major transport of calciclastic deposits occur during sea-level highstands in the form of turbidity flows.

The shoreline transgression during the Early Miocene, to a position far from the shelf edge restricted the influx of siliciclastic sediment onto the continental shelf, suggesting that carbonate sediment was the predominant type feeding PAMA's deep-water basins at that time. As described earlier, channel *y* is only observed in Horizon H₁ and does not continue upwards in Unit 1. Our interpretation is that, unlike the calciclastic submarine fan *a*, there was no effective funnelling system feeding channel *y* above horizon H₁, leading to its abandonment (Figs.7-9).

Based on the data from Soares et al. (2007) and Rossetti et al. (2013), we interpret the middle Miocene (Unit 2) as a falling stage in sea level. Soares et al. (2007) suggested that there is an unconformity in well and seismic data correlating with a marked sea level drop that occurred in PAMA before the late Miocene (Rossetti et al., 2013). In the study area, Horizon H₃ is interpreted being the unconformity described in Soares et al. (2007), separating moderate-to-high-amplitude seismic reflections from low-amplitude strata above (Figs. 3b and 9). At the level of horizon H₃, tributary channel-levee systems were first developed within the calciclastic submarine fan, with channel *a* constituting the main sediment conduit (Fig. 7g, h). The development of tributary channels suggests that sediment supply was significant at the time, although relatively smaller in volume when compared to strata at the level of horizon H₁. This interpretation is also corroborated by a decrease in size of the calciclastic submarine fan in younger strata, until the fan disappears near the modern seafloor. Conversely, a considerable growth of channel *a* is still recorded within the submarine fan until one reaches the modern sea floor, where the channel becomes the predominant feature (Figs. 2, 7 and 10).

Channel *c* started developing at the level of horizon H₂ (Fig. 7i, j). This channel is important as it shows a constant aggradation towards younger strata (Fig. 8). The aggradation of channel *c*, accompanying its lateral migration, suggests that sediment input to the channel was constant regardless of any relative changes in sea level; geomorphic parameters such as cross-sectional area and bankfull width reveal that channel *c* continued to grow over time (Fig.10). Horizon H₃, correlating with the relative drop in the sea level documented in Soares et al. (2007), also reveals that channel *c* did not stop developing at this time, and its geometry remained constant. In addition, Soares et al. (2007) suggest that at the end of the late Miocene and Pliocene (Sequence N40-N50), both the carbonate shelf and associated coastal depositional systems prograded over the PAMA Basin, a character justifying why channel *c* remained active during the deposition of Unit 3.

The continuous development of channel *c* during successive sea-level high- and lowstands, together with its constant sinuosity values through time, prove that calciclastic depositional systems are not primarily controlled by sea-level change, as also suggested in Payros and Pujalte (2008). A possible explanation to the observed aggradation of channel *c* through multiple fluctuations in sea level is the existence of an efficient funnelling mechanism on the continental slope (Fig. 7). Additionally, as described in Jorry et al. (2020), calciclastic sediments can be shed to deep-water systems not just during sea-level highstands, but also during lowstands. Calciclastic sediments might have accumulated on terraces at the slope, to be later redeposited during falling-stages and lowstands in sea-level (Fig. 7).

9.2 Geomorphic characteristics of carbonate deep-water levee-channels

Geomorphic analyses of deep-water channel-levee systems fed by siliciclastic sediment have been previously documented in Lemay et al. (2020) and compared to fluvial channels. It

was recognised that submarine channels are one to two orders of magnitude wider and deeper than fluvial channels, with the latter being more sinuous than submarine channels (Lemay et al., 2020). In this work, we determine how similar calciclastic levee-channels are in comparison to their siliciclastic counterparts.

Based on our results and comparison with published power-law relationships, we can confirm that bankfull width vs. depth relationships of calciclastic channels in PAMA are similar and comparable to siliciclastic channels (Fig. 11a, b). However, calciclastic channels are deeper than siliciclastic channels for a given bankfull width (Fig. 11a, b). Calciclastic channels also appear to be slightly more sinuous than siliciclastic channels as the regression curve between meander amplitude and wavelength is less steep (Fig. 11c, d). Sinuosity values recorded in channel *y* approaches the sinuosity of meandering fluvial channels, marking a distinction with other channels (Fig. 11c). In fact, three different types of calciclastic sediment conduits have been observed in the PAMA Basin: i) Type 1, which are channel-levee systems related to calciclastic submarine fans (channel *a*), ii) Type 2, comprising low sinuosity channel-levee systems *b*, *c* and *x*, and iii) Type 3, which is represented by highly sinuous channel *y* (Fig.12).

9.2.1 *Type 1 – channels related to calciclastic submarine fans*

The early stages of this type of channel are associated with erosive turbidity currents developing furrows within a calciclastic submarine fan (Fig. 12a). These furrows are recognised in cross-sectional data and on key seismic reflectors as small spikes, which mark the loci of incision of erosive turbidity currents (Fig. 12b). As the incision of the furrows continues, a channel-levee system may develop, such as channel *a* (Fig. 12c, d). This type of

channel is characterised by its low sinuosity, and by presenting geomorphic features similar to its siliciclastic counterparts (Fig. 11).

9.2.2 *Type 2 – low sinuosity, aggradational channels*

Type 2 channels record low sinuosity values, usually less than 1.3 (Figs.10 and 12e). Type 2 channels are not associated with calciclastic submarine fans and originate due to the funnelling of sediment from upper slope canyons to form, downslope, a well-defined sediment conduit (Fig. 12h). They start as small channels with high-amplitude internal reflections (Fig. 12f). Due to the characteristic mixing of carbonate and siliciclastic deposits through multiple episodes of sea-level rise and fall, aggradational features are observed in their interior, leading to the generation of large channel-levee systems (Fig. 12g, h).

9.2.3 *Type 3 – high-sinuosity channels*

The high sinuosity (average of 1.4) of Type 3 channels is comparable to fluvial channels (Figs. 10b, 11b and 12i). Channel y shows features such as abandoned channels that suggest a change in its flow direction (Fig. 12i, j). In contrast to the previous low sinuosity channels (Type 2), the cross-sectional area of Type 3 channels is considerably smaller (Fig. 10). This type of channel does not aggrade over time, implying that sediment sources were episodic and not continuous.

10 Conclusions

The main conclusions concerning the deep and ultra-deep mixed calciclastic-siliciclastic depositional systems of the Miocene-Holocene PAMA Basin can be summarised as follows:

- a) We postulate that a portion of the Miocene-Holocene strata of the Travosas Formation comprises a mixed calciclastic-siliciclastic depositional system recording a dominant carbonate input from the continental shelf. A calciclastic submarine fan and channel-levee systems are identified within deep and ultra-deep waters of the PAMA Basin.
- b) Multispectral satellite data point out to a dynamic sediment transport on a mixed calciclastic-siliciclastic carbonate shelf. The PAMA continental shelf is divided into a mixed carbonate-siliciclastic zone in its inner part, and an autochthonous carbonate zone in its middle and outer zones.
- c) Geomorphologic relationships of the PAMA calciclastic channel-levee systems show similarities with modern siliciclastic submarine channel models previously published by Lemay et al. (2020).
- d) The formation of a large calciclastic submarine fan in the lower Miocene correlates with a period of progradation and lateral growth of the carbonate shelf during a sea-level rise. Erosional furrows are characteristic of distal fans, and comprise an effective funnelling mechanism for younger channels forming on the continental slope.
- e) Three different types of deep-water depositional systems are recognised in the PAMA Basin: channels related to calciclastic submarine fans (Type 1), low sinuosity-aggradational channels (Type 2), and high sinuosity channels (Type 3).
- f) Channels related to calciclastic submarine fans (Type 1), such as channel *a*, were initiated by the action of highstand turbidity flows. The continuous erosive turbidite flows led to an increase in the funnelling of sediment, developing a large channel-levee system.
- g) Low-sinuosity channels (Type 2) are not associated with calciclastic submarine fans, are aggradational, and appear to develop through time regardless of any relative sea-level change. This can be explained by the accumulation of sediment in topographic

features, such as terraces on the continental slope, which is later redeposited during sea-level lowstands. Furthermore, the presence of a steepened ramp on the PAMA continental shelf provides a continuous supply of carbonate material during sea-level lowstands as the productive zone shifts basinwards.

- h) Highly sinuous channels (Type 3) are characterised by their small cross-sectional area, showing a bankfull wavelength vs. amplitude relationship, and sinuosity values, that are similar to fluvial channels.

11 Acknowledgements

The work contained in this paper is part of a PhD research supported by the Mexican National Council of Science and Technology (CONACYT) and the hydrocarbon Secretariat of Energy (SENER). Polarcus is acknowledged to provide the Pará-Maranhão 3D seismic volume as well as Schlumberger Petrel® and ESRI ArcGIS® for granting academic licenses to Cardiff's 3D Seismic Lab. The authors acknowledge the Brazilian National Agency of Petroleum, Natural Gas and Biofuels (ANP) for the well data provided. We thank Martin Lemay for sharing the Python scripts used for the channel planform measurements as well as the data for modern siliciclastic sediment conduits. We also would like to thank Basin Research Editor, Peter Burgess and reviewers Lorena Moscardelli and Xavier Janson for their useful and constructive comments.

12 References

- Aguilera, O., Oliveira de Araújo, O.M., Hendy, A., Nogueira, A.A.E., Nogueira, A.C.R., Maurity, C.W., Kutter, V.T., Martins, M.V.A., Coletti, G., Dias, B.B., da Silva-Caminha, S.A.F., Jaramillo, C., Bencomo, K., Lopes, R.T., 2020. Palaeontological framework from Pirabas Formation (North Brazil) used as potential model for equatorial carbonate platform. *Marine Micropaleontology* 154, 101813.
- Almeida, N.M. De, Alves, T.M., Filho, F.N., Souza, A.C.B., Oliveira, K.M.L., Barbosa, T.H.S., 2020. A three-dimensional (3D) structural model for an oil-producing basin of the Brazilian Equatorial margin. *Marine and Petroleum Geology*.
- Almeida, N., Alves, T., Filho, N., Freire, S., de Souza, C., Leopoldino, K., Normando, M., Barbosa, T., 2018. Tectono-sedimentary evolution and petroleum system of a new deep-water exploration frontier: Mundaú sub-basin Equatorial Brazil. *AAPG Bulletin* 0, 20.
- Alves, T., Fetter, M., Busby, C., Gontijo, R., Cunha, T.A., Mattos, N.H., 2020. A tectono-stratigraphic review of continental breakup on intraplate continental margins and its impact on resultant hydrocarbon systems., *Marine and Petroleum Geology*.
- Alves, T.M., Abreu Cunha, T., 2018. A phase of transient subsidence, sediment bypass and deposition of regressive–transgressive cycles during the breakup of Iberia and Newfoundland. *Earth and Planetary Science Letters* 484, 168–183.
- Andresen, N., Reijmer, J.J.G., Droxler, A.W., 2003. Timing and distribution of calciturbidites around a deeply submerged carbonate platform in a seismically active setting (Pedro Bank, Northern Nicaragua Rise, Caribbean Sea). *International Journal of Earth Sciences* 92, 573–592.
- Aquino da Silva, A.G., Amaro, V.E., Stattegger, K., Schwarzer, K., Vital, H., Heise, B., 2015.

- 863 Spectral calibration of CBERS 2B multispectral satellite images to assess suspended
864 sediment concentration. *ISPRS Journal of Photogrammetry and Remote Sensing* 104, 53–
865 62.
- 866 Back, S., Reuning, L., 2015. Channels in Carbonate Environments: 3-D-Seismic
867 Characteristics Extracted From the Sedimentary Record. AAPG Annual Convention and
868 Exhibition, Denver, Co.
- 869 Baker, E., Gaill, F., Karageorgis, A., Lamarche, G., Narayanaswamy, B., Parr, J.,
870 Raharimananirina, C., Santos, R., Sharma, R., Tuhumwire, J., 2016. Offshore mining
871 industries. In: (UN), U.N. (Ed.), *The First Global Integrated Marine Assessment; World*
872 *Ocean Assessment I*. New York, NY, USA.
- 873 Betzler, C., Lindhorst, S., Eberli, G.P., Lüdman, T., Möbius, J., Ludwig, J., Schutter, I.,
874 Wunsch, M., Reijmer, J.J.G., Hübscher, C., 2014. Periplatform drift: The combined result
875 of contour current and off-bank transport along carbonate platforms. *Geology* 42, 871–
876 874.
- 877 Betzler, C., Reijmer, J.J.G., Bernetà, K., Eberlià, G.P., Anselmetti, F.S., 1999. Sedimentary
878 patterns and geometries of the Bahamian outer carbonate ramp (Miocene±Lower
879 Pliocene, Great Bahama Bank). *Sedimentology* 46.
- 880 Bornhold, B.D., Pilkey, O.H., 1971. Bioclastic turbidite sedimentation in Columbus Basin,
881 Bahamas. *Bulletin of the Geological Society of America* 82, 1341–1354.
- 882 Braga, J.C., Martin, J.M., Wood, J.L., 2001. Submarine lobes and feeder channels of
883 redeposited, temperate carbonate and mixed siliciclastic-carbonate platform deposits
884 (Vera Basin, Almería, southern Spain).
- 885 Brandão, J., Feijó, F.J., 1994. Bacia do Pará-Maranhão. *Boletim de Geociências Da*

- 886 PETROBRÁS 8, 101–102.
- 887 Catuneanu, O., 2006. Principles of sequence stratigraphy. Elsevier.
- 888 Chiarella, D., Longhitano, S.G., Tropeano, M., 2017. Types of mixing and heterogeneities in
889 siliciclastic-carbonate sediments. *Marine and Petroleum Geology* 88, 617–627.
- 890 Clare, M.A., Vardy, M.E., Cartigny, M.J.B., Talling, P.J., Himsworth, M.D., Dix, J.K., Harris,
891 J.M., Whitehouse, R.J.S., Belal, M., 2017. Direct monitoring of active geohazards:
892 Emerging geophysical tools for deep-water assessments. *Near Surface Geophysics* 15,
893 427–444.
- 894 Coniglio, M., Dix, G.R., 1992. Carbonate Slopes. In: Walker, R.G., James, N.P. (Eds.), *Facies*
895 *Models–Response to Sea-Level Change*. Geological Association of Canada, St. John's
896 Newfoundland.
- 897 Counts, J.W., Jorry, S.J., Vazquez Riveiros, N., Jouet, G., Giraudeau, J., Cheron, S., Boissier,
898 A., Miramontes, E., 2019. A Late Quaternary record of highstand shedding from an
899 isolated carbonate platform (Juan de Nova, southern Indian Ocean). *The Depositional*
900 *Record* 5, 540–557.
- 901 Crevello, P.D., Schlager, W., 1980. Carbonate debris sheets and turbidites, Exuma Sound,
902 Bahamas. *Journal of Sedimentary Petrology* 50, 1121–1148.
- 903 Cross, T.A., Lessenger, M.A., 1988. Seismic Stratigraphy. *Annual Review of Earth and*
904 *Planetary Sciences* 16, 319–354.
- 905 Da Silva, B., Ribeiro, H.J.P.S., 2018. Exploratory plays of Pará-Maranhão and Barreirinhas
906 basins in deep and ultra-deep waters, Brazilian Equatorial Margin. *Brazilian Journal of*
907 *Geology* 48, 485–502.
- 908 Da Silva, C.P., 2007. Estudo Sobre Foraminíferos e Radiolários do Cretáceo, Bacia Pará-

- 909 Maranhão, Margem Equatorial Brasileira. Universidade Federal do Rio Grande do Sul.
- 910 de Moraes, J.O., Ximenes Neto, A.R., Pessoa, P.R.S., de Souza Pinheiro, L., 2019.
- 911 Morphological and sedimentary patterns of a semi-arid shelf, Northeast Brazil. Geo-
- 912 Marine Letters 40, 1–8.
- 913 De Souza, V., 2006. Radiolários Do Cretáceo Médio Das Bacias Do Pará-Maranhão E
- 914 Barreirinhas, Margem Equatorial Brasileira Vladimir. Universidade Federal do Rio
- 915 Grande do Sul.
- 916 Dias, F.J.S., Castro, B.M., Lacerda, L.D., 2013. Continental shelf water masses off the
- 917 Jaguaribe River (4S), northeastern Brazil. Continental Shelf Research 66, 123–135.
- 918 Ditty, P.S., Harmon, C.J., Pilkey, O.H., Ball, M.M., Richardson, E.S., 1977. Mixed
- 919 terrigenous-Carbonate sedimentation in the Hispaniola-Caicos turbidite basin. Marine
- 920 Geology 24, 1–20.
- 921 Droxler, A.W., Schlager, W., 1985. Glacial versus interglacial sedimentation rates and turbidite
- 922 frequency in the Bahamas. Geology 13, 799–802.
- 923 Dunlap, D., Janson, X., Sanchez Phelps, C., Covault, J., 2018. Carbonate Channel-Levee
- 924 Systems Influenced by Mass-Transport Complexes, Browse Basin, Western Australia.
- 925 AAPG ACE 2018.
- 926 Eberli, G.P., Anselmetti, F.S., Betzler, C., Van Konijnenburg, J.H., Bernoulli, D., 2005.
- 927 Carbonate platform to basin transitions on seismic data and in outcrops: Great Bahama
- 928 Bank and the Maiella Platform margin, Italy. AAPG Memoir 207–250.
- 929 Eberli, G.P., Swart, P.K., McNeill, D.F., Kenter, J.A.M., Anselmetti, F.S., Melim, L.A.,
- 930 Ginsburg, R.N., 1997. A synopsis of the Bahamas Drilling Project: results from two deep
- 931 core borings drilled on the Great Bahama Bank. In: Marin, J.A. (Ed.), Proceedings of the

- 932 Ocean Drilling Program, Initial Reports. Ocean Drilling Program, Texas A&M
933 University, 23–41.
- 934 Fabianovicz, R., 2013. Pará-Maranhão Basin. Brasil 11th Round - Oil & Gas Bidding Rounds.
935 National Agency of Petroleum, Natural Gas and Biofuels, Rio de Janeiro.
- 936 Figueiredo, J.D.J.P. De, Zalán, P.V., Soares, E.F., 2007. Bacia da Foz do Amazonas. Boletim
937 de Geociencias - Petrobras 15, 299–309.
- 938 Francis, J.M., Daniell, J.J., Droxler, A.W., Dickens, G.R., Bentley, S.J., Peterson, L.C.,
939 Opdyke, B.N., Beaufort, L., 2008. Deep water geomorphology of the mixed siliciclastic-
940 carbonate system, Gulf of Papua. Journal of Geophysical Research: Earth Surface 113, 1–
941 22.
- 942 Gallagher, S.J., Smith, A.J., Jonasson, K., Wallace, M.W., Holdgate, G.R., Daniels, J., Taylor,
943 D., 2001. The miocene palaeoenvironmental and palaeoceanographic evolution of the
944 gippsland basin, southeast australia: A record of southern ocean change.
945 Palaeogeography, Palaeoclimatology, Palaeoecology 172, 53–80.
- 946 Gee, M.J.R., Gawthorpe, R.L., Bakke, K., Friedmann, S.J., 2007. Seismic geomorphology and
947 evolution of submarine channels from the Angolan continental margin. Journal of
948 Sedimentary Research 77, 433–446.
- 949 Glaser, K.S., Droxler, A.W., 1993. Controls and Development of Late Quaternary Periplatform
950 Carbonate Stratigraphy in Walton Basin (Northeastern Nicaragua Rise, Caribbean Sea).
951 Paleoceanography 8, 243–274.
- 952 Gradstein, F.M., Ogg, J.G., Smith, A.G., 2005. A geologic time scale 2004, A Geologic Time
953 Scale 2004. Cambridge University Press.
- 954 Hedley, J.D., Roelfsema, C., Brando, V., Giardino, C., Kutser, T., Phinn, S., Mumby, P.J.,

- 955 Barrilero, O., Laporte, J., Koetz, B., 2018. Coral reef applications of Sentinel-2: Coverage,
956 characteristics, bathymetry and benthic mapping with comparison to Landsat 8. Remote
957 Sensing of Environment 216, 598–614.
- 958 Held, A., 2011. Apport de la paléohydrologie dans la quantification des rôles respectifs du
959 climat et de la tectonique des systèmes fluviaux méandriiformes fossiles : application à
960 des systèmes oligo-miocènes d ' Europe occidentale To cite this version : HAL Id : paste,
961 <http://www.theses.fr>. Paris, ENMP.
- 962 Henry, S., Kumar, N., Danforth, A., Nuttall, P., Venkatraman, S., 2011. Ghana-Sierra Leone
963 Lookalike Plays in Northern Brazil. GeoExPro 8, 36–41.
- 964 James, N.P., Mountjoy, E.W., 1983. Shelf-slope break in fossil carbonate platforms: an
965 overview. In: Stanley, D.J., Moore, G.T. (Eds.), The Shelfbreak: Critical Interface on
966 Continental Margins. SEPM Special Publication, 33. SEPM Society for Sedimentary
967 Geology, 189–206.
- 968 Janson, X., Dunlap, D., Zeng, L., Sanchez Phelps, C., Covault, J., 2018. Carbonate Shelf to
969 Basin Architecture and Slope Seismic Geomorphology, Lower Miocene, Browse Basin,
970 Northwest Shelf of Australia. AAPG ACE 2018.
- 971 Jorry, S.J., Droxler, A.W., Mallarino, G., Dickens, G.R., Bentley, S.J., Beaufort, L., Peterson,
972 L.C., Opdyke, B.N., 2008. Bundled turbidite deposition in the central Pandora Trough
973 (Gulf of Papua) since Last Glacial Maximum: Linking sediment nature and accumulation
974 to sea level fluctuations at millennial timescale. Journal of Geophysical Research: Earth
975 Surface 113, 1–15.
- 976 Jorry, S.J., Jouet, G., Edinger, E.N., Toucanne, S., Counts, J.W., Miramontes, E., Courgeon,
977 S., Riveiros, N.V., Le Roy, P., Camoin, G.F., 2020. From platform top to adjacent deep
978 sea: New source-to-sink insights into carbonate sediment production and transfer in the

- 979 SW Indian Ocean (Glorieuses archipelago). Marine Geology.
- 980 Kang, H., Meng, J., Cheng, T., Jia, H., Bai, B., Li, M., 2018. Characteristics of deep water
981 depositional system in Campos basin, Brazil. Petroleum Exploration and Development
982 45, 99–110.
- 983 Kendall, C.G.S.C., Schlager, W., 1981. Carbonates and relative changes in sea level. Marine
984 Geology 44, 181–212.
- 985 Kenter, J.A.M., 1990. Carbonate platform flanks: slope angle and sediment fabric.
986 Sedimentology 37, 777–794.
- 987 Lemay, M., Grimaud, J.L., Cojan, I., Rivoirard, J., Ors, F., 2020. Geomorphic variability of
988 submarine channelized systems along continental margins: Comparison with fluvial
989 meandering channels. Marine and Petroleum Geology 115, 104295.
- 990 Ma, B., Wu, S., Mi, L., Lüdmann, T., Gao, J., Gao, W., 2018. Mixed Carbonate-Siliciclastic
991 Deposits in a Channel Complex in the Northern South China Sea. Journal of Earth Science
992 29, 707–720.
- 993 Milliman, J.D., 1993. Production and accumulation of calcium carbonate in the ocean: budget
994 of a nonsteady state. Global Biogeochemical Cycles 7, 927–957.
- 995 Moscardelli, L., Ochoa, J., Hunt, I., Zahm, L., 2019. Mixed siliciclastic–carbonate systems and
996 their impact for the development of deep-water turbidites in continental margins: A case
997 study from the Late Jurassic to Early Cretaceous Shelburne subbasin in offshore Nova
998 Scotia. AAPG Bulletin 103, 2487–2520.
- 999 Mulder, T., Ducassou, E., Gillet, H., Hanquiez, V., Principaud, M., Chabaud, L., Eberli, G.P.,
1000 Kindler, P., Billeaud, I., Gonthier, E., Fournier, F., Leonide, P., Borgomano, J., 2014. First
1001 Discovery of Channel-Levee Complexes In A Modern Deep-Water Carbonate Slope

- 1002 Environment. *Journal of Sedimentary Research* 84, 1139–1146.
- 1003 Mulder, T., Ducassou, E., Gillet, H., Hanquiez, V., Tournadour, E., Combes, J., Eberli, G.P.,
1004 Kindler, P., Gonthier, E., Conesa, G., Robin, C., Sianipar, R., Reijmer, J.J.G., François,
1005 A., 2012. Canyon morphology on a modern carbonate slope of the bahamas: Evidence of
1006 regional tectonic tilting. *Geology* 40, 771–774.
- 1007 Nemčok, M., Henk, A., Allen, R., Sikora, P.J., Stuart, C., 2013. Continental break-up along
1008 strike-slip fault zones; observations from the equatorial Atlantic. *Geological Society*
1009 *Special Publication* 369, 537–556.
- 1010 Oliveira, M.J.R., Santarem, P., Moraes, A., Zalán, P. V., Caldeira, J.L., Tanaka, A., Trosdtorf,
1011 I., 2012. Linked extensional-compressional tectonics in gravitational systems in the
1012 equatorial margin of Brazil. *AAPG Memoir* 159–178.
- 1013 Payros, A., Pujalte, V., 2008. Calciclastic submarine fans: An integrated overview., *Earth-*
1014 *Science Reviews*.
- 1015 Payros, A., Pujalte, V., Orue-Etxebarria, X., 2007. A point-sourced calciclastic submarine fan
1016 complex (Eocene Anotz Formation, western Pyrenees): facies architecture, evolution and
1017 controlling factors. *Sedimentology* 54, 137–168.
- 1018 Pettingill, H.S., 2006. Global Overview of Deepwater Exploration and Production. In: Weimer,
1019 P., Slatt, R.M., Bouroullec, R., Fillon, R., Pettingill, H., Pranter, M., Tari, G. (Eds.),
1020 Introduction to the Petroleum Geology of Deepwater Setting. American Association of
1021 Petroleum Geologists (AAPG).
- 1022 Piovesan, E.K., 2008. Ostracodes Cretáceos (Turoniano-Maastrichtiano) Da Bacia Do Pará-
1023 Maranhão: Aspectos Taxonômicos, Paleoecológicos E Paleobiogeográficos.
1024 Universidade do Vale do Rio dos Sinos.

- 1025 Playton, T.E., Janson, X., Kerans, C., 2010. Carbonate Slopes. In: James, N., Dalrymple, R.W.
1026 (Eds.), Facies Models 4. Geological Association of Canada, St. Johns, Newfoundland,
1027 449–476.
- 1028 Puga-Bernabéu, Á., Webster, J.M., Beaman, R.J., Reimer, P.J., Renema, W., 2014. Filling the
1029 gap: A 60ky record of mixed carbonate-siliciclastic turbidite deposition from the Great
1030 Barrier Reef. *Marine and Petroleum Geology* 50, 40–50.
- 1031 Rankey, E.C., 2017. Seismic architecture and seismic geomorphology of heterozoan
1032 carbonates: Eocene-Oligocene, Browse Basin, Northwest Shelf, Australia. *Marine and*
1033 *Petroleum Geology* 82, 424–443.
- 1034 Ravenne, C., Vially, R., Francaise, C., Valery, P., 1985. Deep Clastic Carbonate Deposits of
1035 the Bahamas — Comparison With Mesozoic Outcrops of the Vercors and Vocontian
1036 Trough.
- 1037 Reijmer, J.J.G., Andresen, N., 2007. Mineralogy and grain size variations along two carbonate
1038 margin-to-basin transects (Pedro Bank, Northern Nicaragua Rise). *Sedimentary Geology*
1039 198, 327–350.
- 1040 Reijmer, J.J.G., Mulder, T., Borgomano, J., 2015a. Carbonate slopes and gravity deposits.
1041 *Sedimentary Geology* 317, 1–8.
- 1042 Reijmer, J.J.G., Palmieri, P., Groen, R., 2012. Compositional variations in calciturbidites and
1043 calcidebrites in response to sea-level fluctuations (Exuma Sound, Bahamas). *Facies* 58,
1044 493–507.
- 1045 Reijmer, J.J.G., Palmieri, P., Groen, R., Floquet, M., 2015b. Calciturbidites and calcidebrites:
1046 Sea-level variations or tectonic processes? *Sedimentary Geology* 317, 53–70.
- 1047 Rinke-Hardekopf, L., Reuning, L., Bourget, J., Back, S., 2018. Syn-sedimentary deformation

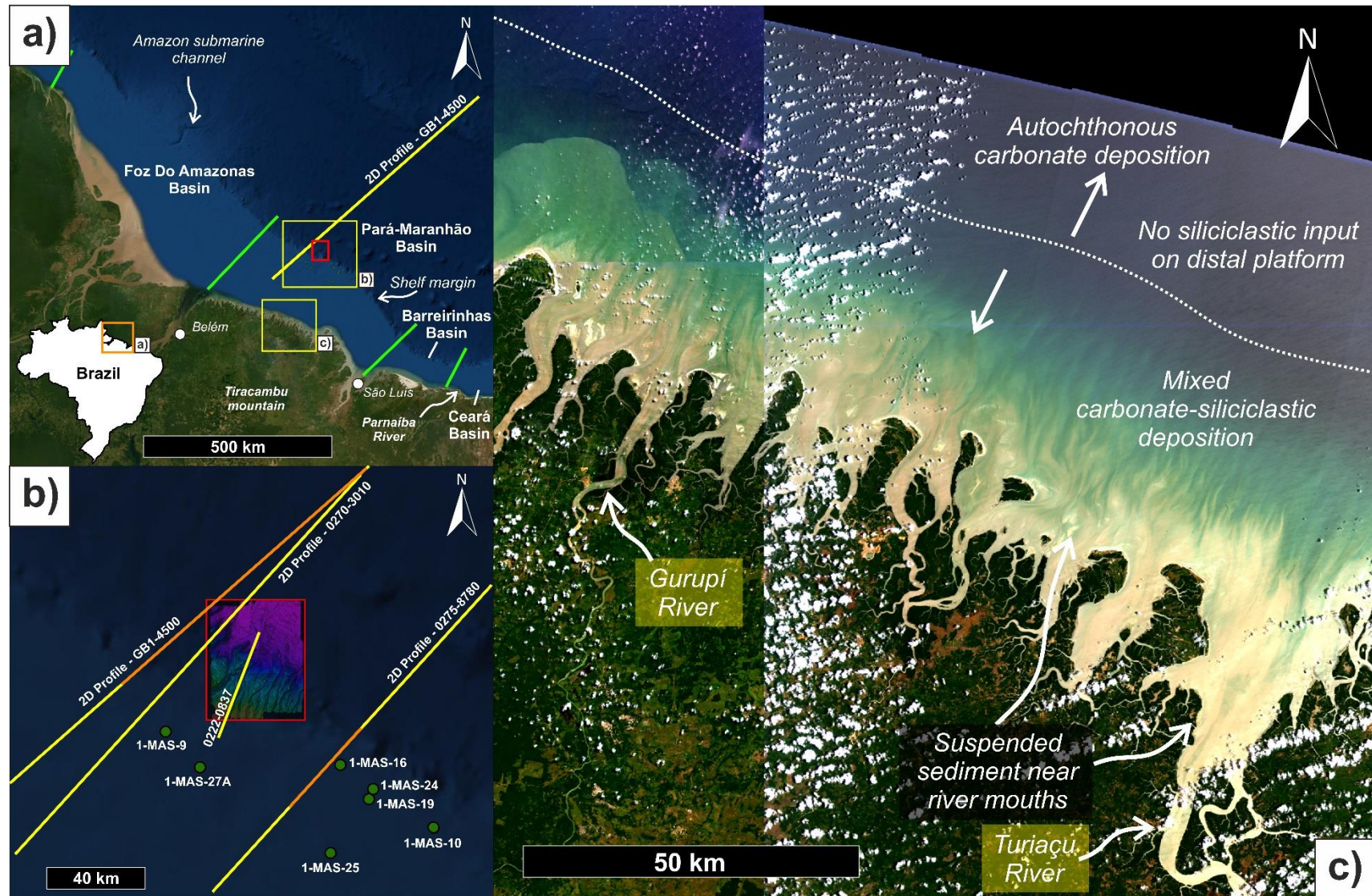
- 1048 as a mechanism for the initiation of submarine gullies on a carbonate platform to slope
1049 transition, Browse Basin, Australian North West Shelf. *Marine and Petroleum Geology*
1050 91, 622–630.
- 1051 Rossetti, D.F., Bezerra, F.H.R., Dominguez, J.M.L., 2013. Late oligocene-miocene
1052 transgressions along the equatorial and eastern margins of brazil. *Earth-Science Reviews*
1053 123, 87–112.
- 1054 Savitzky, A., Golay, M.J.E., 1964. Smoothing and differentiation of data by simplified least
1055 squares procedures. *Analytical Chemistry* 36, 1627–1639.
- 1056 Schneider, J.A., Senders, M., 2010. Foundation design: A comparison of oil and gas platforms
1057 with offshore wind turbines. *Marine Technology Society Journal* 44, 32–51.
- 1058 Soares, D.M., Alves, T.M., Terrinha, P., 2012. The breakup sequence and associated
1059 lithospheric breakup surface: Their significance in the context of rifted continental
1060 margins (West Iberia and Newfoundland margins, North Atlantic). *Earth and Planetary*
1061 *Science Letters* 355–356, 311–326.
- 1062 Soares, E.F., Zalán, P.V., Figueiredo, J.J.P., Trosdorf Jr, I., 2007. Bacia do Pará-Maranhão.
1063 *Boletim de Geociências Da Petrobras* 15, 321–330.
- 1064 Soares Júnior, A.V., 2002. Paleografia e evolução da paisagem do nordeste do estado do Pará
1065 e noroeste do Maranhão: cretáceo ao holoceno, Arsyad, Azhar,. Universidade Federal do
1066 Pará.
- 1067 Soares Júnior, A.V., Hasui, Y., Costa, J.B.S., Machado, F.B., 2011. Evolução do rifteamento e
1068 paleogeografia da margem Atlântica Equatorial do Brasil: Triássico ao Holoceno.
1069 *Geociencias* 30, 669–692.
- 1070 Sylvester, Z., Pirmez, C., 2017. Latitudinal changes in the morphology of submarine channels:

- 1071 Reevaluating the evidence for the influence of the coriolis force. SEPM Special
1072 Publications 108, 82–92.
- 1073 Tesch, P., Reece, R.S., Pope, M.C., Markello, J.R., 2018. Quantification of architectural
1074 variability and controls in an Upper Oligocene to Lower Miocene carbonate ramp, Browse
1075 Basin, Australia. *Marine and Petroleum Geology* 91, 432–454.
- 1076 Tournadour, E., Mulder, T., Borgomano, J., Gillet, H., Chabaud, L., Ducassou, E., Hanquiez,
1077 V., Etienne, S., 2017. Submarine canyon morphologies and evolution in modern carbonate
1078 settings: The northern slope of Little Bahama Bank, Bahamas. *Marine Geology* 391, 76–
1079 97.
- 1080 Trosdorf Junior, I., Zalán, P.V., Figueiredo, J. de J.P. De, Soares, E.F., 2007. Bacia de
1081 Barreirinhas. *Boletim de Geociencias - Petrobras* 15, 331–339.
- 1082 Weimer, P., Slatt, R.M., 2004. Deepwater Reservoir Elements: Channels and their Sedimentary
1083 Fill. In: Weimer, P., Slatt, R. (Eds.), *Petroleum Systems of Deepwater Settings*. Society
1084 of Exploration Geophysicists and European Association of Geoscientists and Engineers.
- 1085 Williams, G.P., 1986. River meanders and channel size. *Journal of Hydrology* 88, 147–164.
- 1086 Wright, V.P., Burchette, T.P., 1998. Carbonate ramps: An introduction. *Geological Society*
1087 Special Publication 149, 1–5.
- 1088 Wunsch, M., Betzler, C., Lindhorst, S., Lüdmann, T., Eberli, G.P., 2017. Sedimentary
1089 dynamics along carbonate slopes (Bahamas archipelago). *Sedimentology* 64, 631–657.
- 1090 Zalán, P.V., 2015. Re-Interpretation of an Ultra-Deep Seismic Section in the Para-Maranhao
1091 Basin - Implications for the Petroleum Potential of the Ultra-Deep Waters. *OTC Brasil*
1092 2015: The Atlantic: From East to West - An Ocean of Innovation. 662–672.
- 1093 Zalán, P.V., 2001. Growth Folding in Gravitational Fold-and-Thrust Belts in the Deep Waters

- 1094 of the Equatorial Atlantic, Northeastern Brazil. Seventh International Congress of the
1095 Brazilian Geophysical Society. AAPG Datapages/Search and Discovery.
- 1096 Zeng, L.Y., 2020. Seismic-based geomorphology of a mixed carbonate siliciclastic shelf-to-
1097 basin submarine drainage system , Miocene , Browse Basin , Northwest Shelf of Australia
1098 APPROVED BY SUPERVISING COMMITTEE : The University of Texas at Austin.
- 1099

1100 13 Figures
1101

FIGURE 1



1102

1103 Figure 1. a) Location map of the Brazilian Equatorial Margin highlighting the study area in the Pará-Maranhão (PAMA) Basin. Red rectangle
1104 shows the location of the studied 3D seismic survey. Green lines mark basin limits. b) Detailed map showing published 2D seismic profiles crossing
1105 the study area, used to correlate the stratigraphy of the interpreted horizons. Profile GB1-4500 is from Henry et al. (2011) and Zalán (2015), profile
1106 0222-0837 is from Fabianovicz (2013) and profiles 0270-3010 and 0275-8780 are taken from Da Silva and Riveiro (2018). Exploration wells near
1107 the interpreted 3D seismic survey are shown as green dots. For the detailed well correlation, please refer to Fig. 5. All wells were drilled in shallow
1108 waters of the carbonate shelf. c) Multispectral satellite (Sentinel-2) map showing a bathymetric band combination using B4-Red, B3-Green and
1109 B1-Ultra blue bands. This map highlights the PAMA offshore areas with suspended siliciclastic sediment and autochthonous carbonate deposits.

FIGURE 2



1113

1114 continental slope, whereas there is a major channel-levee system on the continental rise.
1115 Different sediment conduits are labelled from a to f. Red arrows indicate sediment funnelling
1116 points within the continental slope. Note the high number of funnelling conduits towards
1117 channel *a*.

FIGURE 3

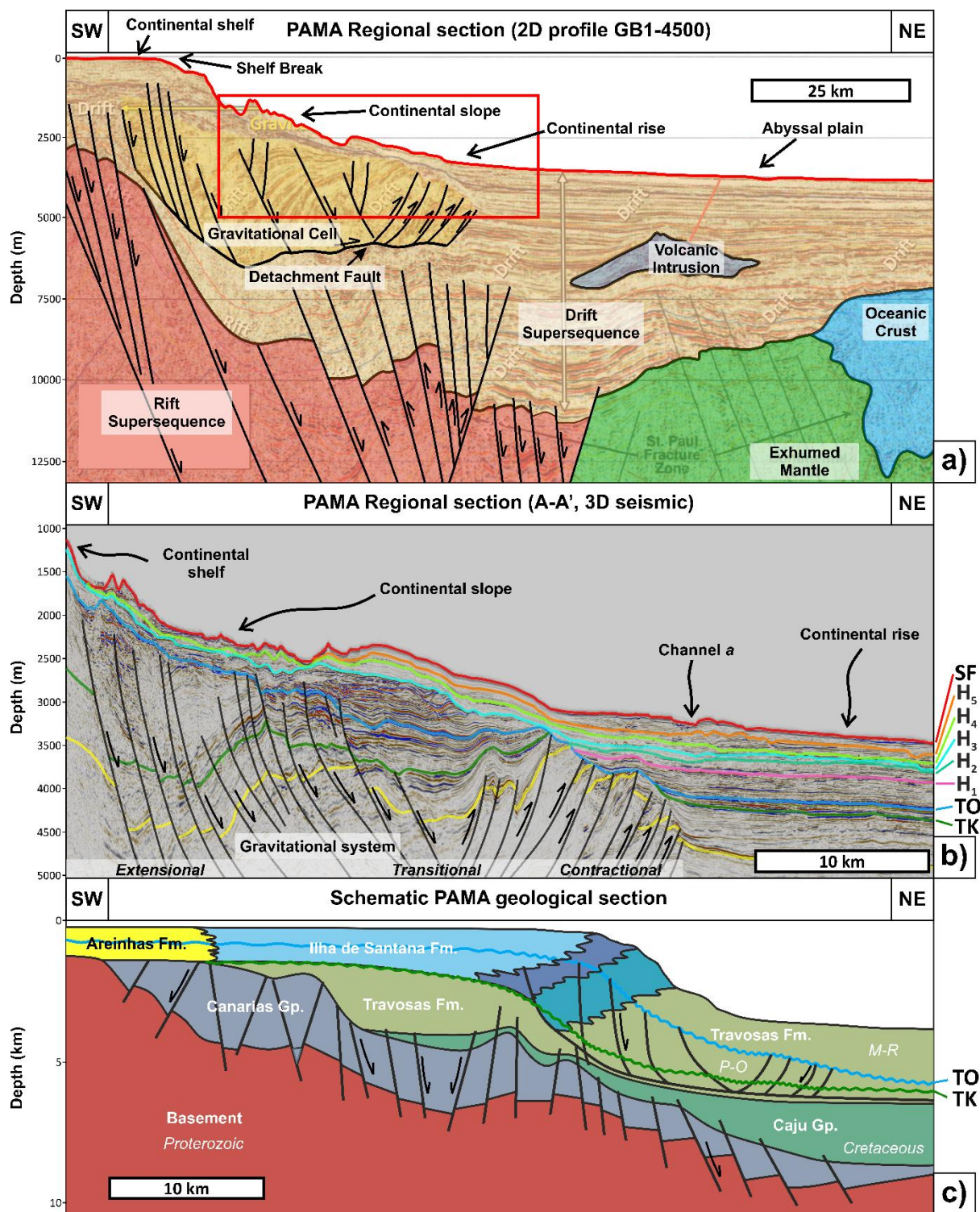


Figure 3. Regional seismic sections depicting the regional stratigraphic units and seismic facies of the PAMA Basin. a) Reinterpreted 2D seismic profile GB1-4500 from Henry et al. (2011) and Zalán (2015) displaying the depositional sequences of the basin at the regional scale. A red

1123 rectangle shows the portion of the basin studied in this work, which encompasses the upper
1124 section of the Drift Supersequence above the gravitational cell. Refer to Fig. 1b for location.
1125 b) Seismic section of the 3D seismic survey showing the detailed stratigraphy of the PAMA
1126 Basin. A gravitational system is observed below the Top Oligocene (TO) unconformity
1127 comprising extensional, transitional and contractional sections. Refer to Fig. 2 for location. c)
1128 Schematic section of the PAMA Basin outlining the distribution of the different geological
1129 formations. P-O=Paleocene-Oligocene, M-R=Miocene-Recent. Modified after Brandão and
1130 Feijó (1994).
1131

FIGURE 4

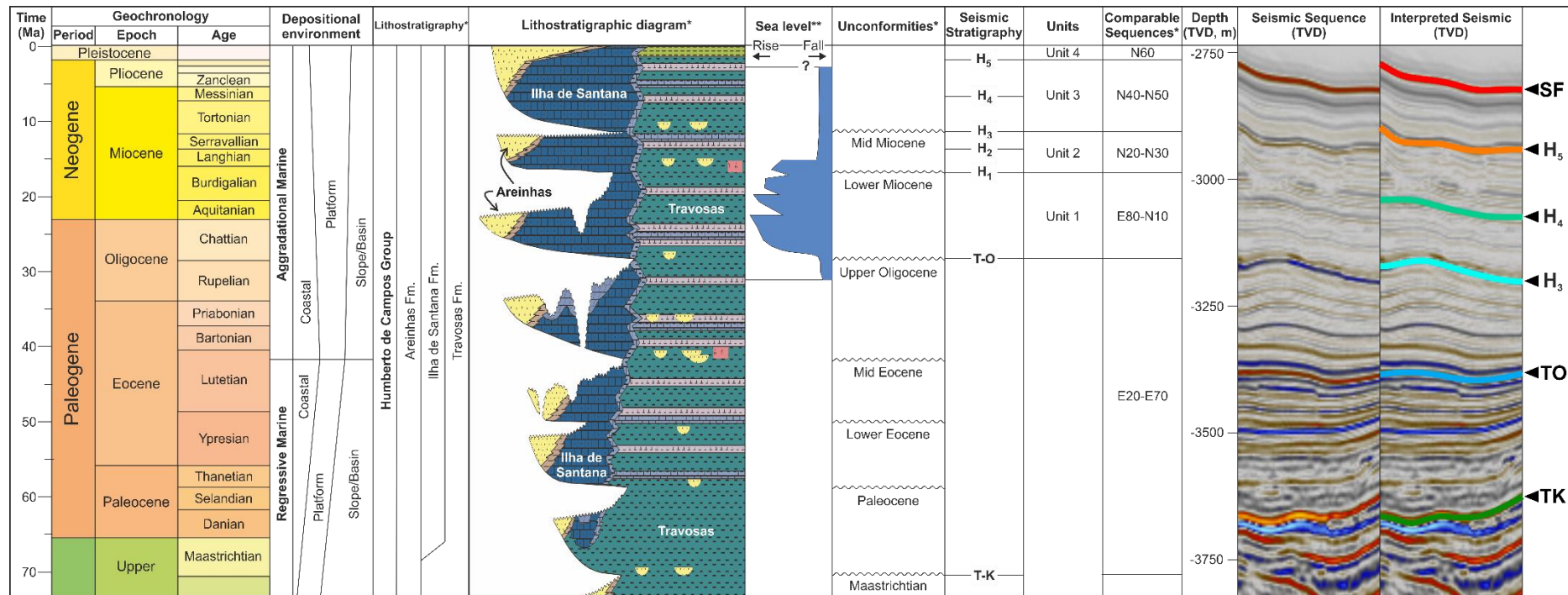
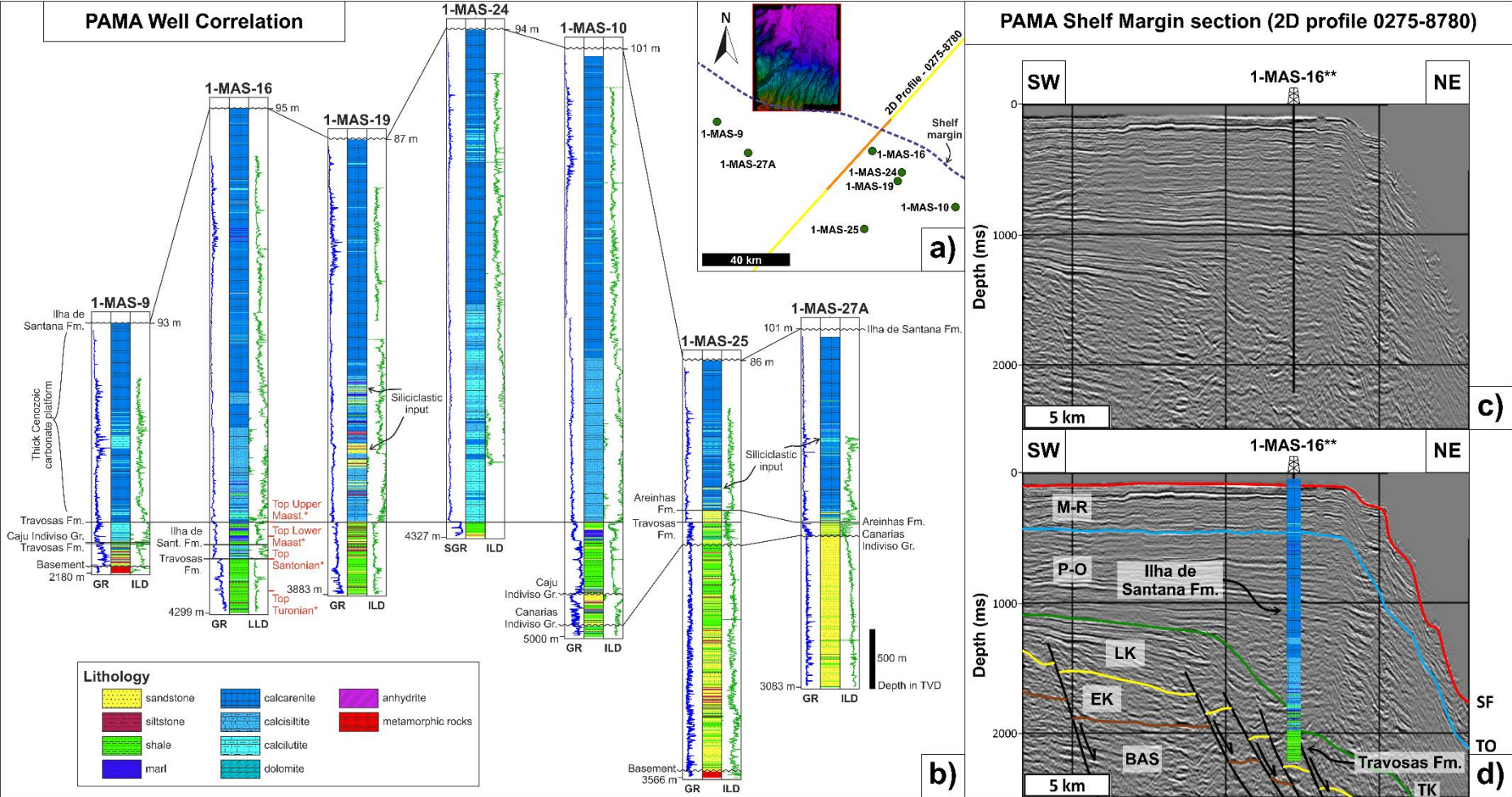


Figure 4. Cenozoic lithostratigraphic chart of the PAMA Basin and its main seismic stratigraphic units. *Comparable sequences, unconformities and lithostratigraphy taken from Soares et al. (2007). **Sea level curve taken from Rossetti et al. (2013) based on data from the Pirabas and Barreiras formations.

FIGURE 5



1139 Figure 5. Well correlation panel and seismic sections on the PAMA shelf margin. a) Map of the study area showing the location of wells and
1140 seismic data. A blue dashed line shows the shelf margin for reference. b) Well correlation panel for wells 1-MAS-9, 1-MAS-16, 1-MAS-19, 1-
1141 MAS-24, 1-MAS-10, 1-MAS-25 and 1-MAS-27A. Well correlation is flattened on the Travosas Formation marker. Information displayed for each
1142 well are lithology, Gamma-Ray (GR) and Deep Resistivity (ILD) wireline curves. *Cretaceous ages for well 1-MAS-16 were taken from
1143 paleontological data in Piovesan (2008). c) and d) Uninterpreted and interpreted seismic profile 0275-8780 showing the PAMA shelf margin with
1144 a thick carbonate platform corresponding to the Ilha de Santana Formation. **Well location is projected. BAS=Basement, EK=Early Cretaceous,
1145 LK=Late Cretaceous, P-O=Paleocene-Oligocene, M-R=Miocene-Recent. Modified from Da Silva and Ribeiro (2018).

1146

1147

FIGURE 6

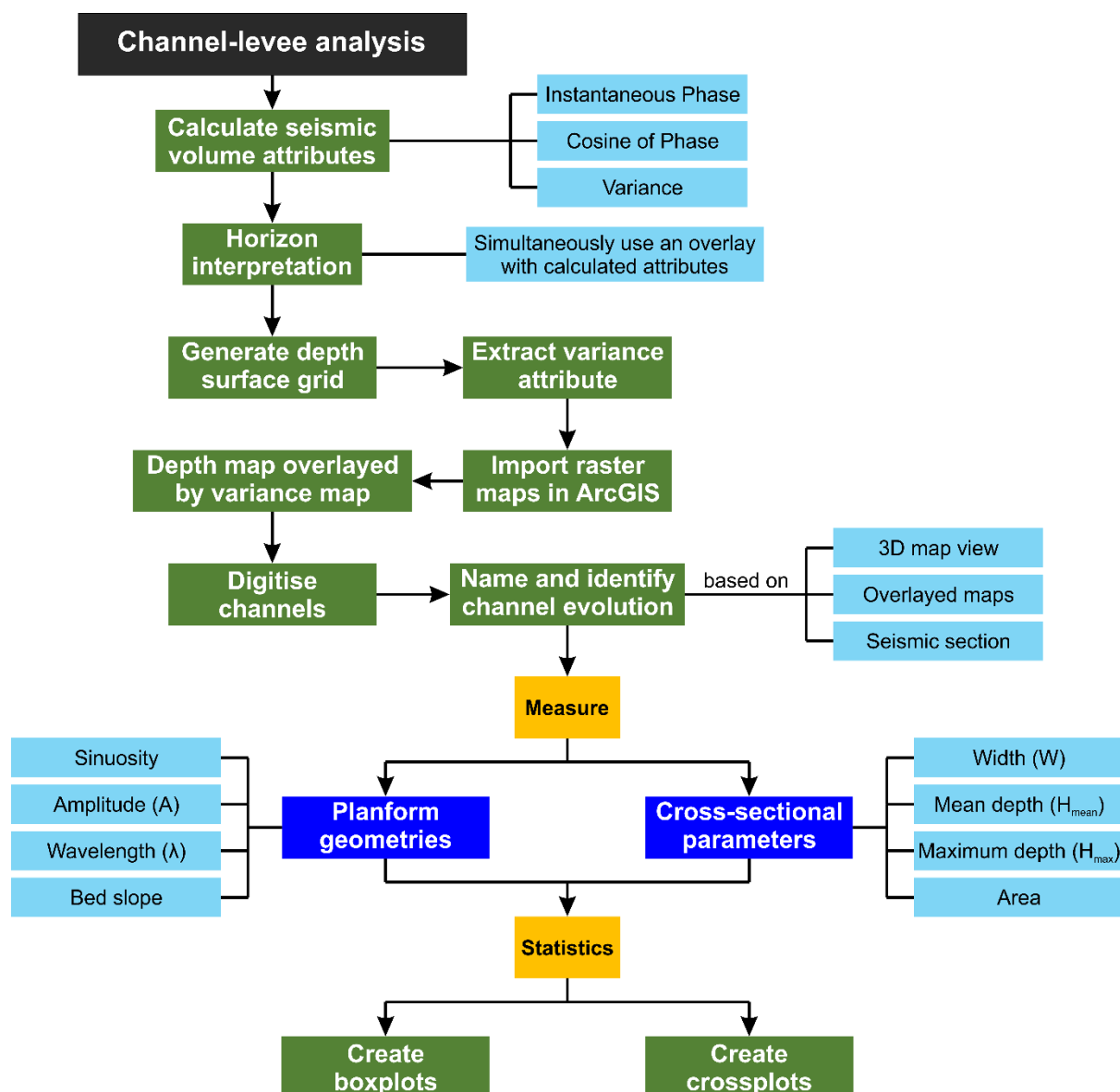


Figure 6. Flowchart summarising the methodology used in this work to identify and analyse channel-levee systems.

FIGURE 7

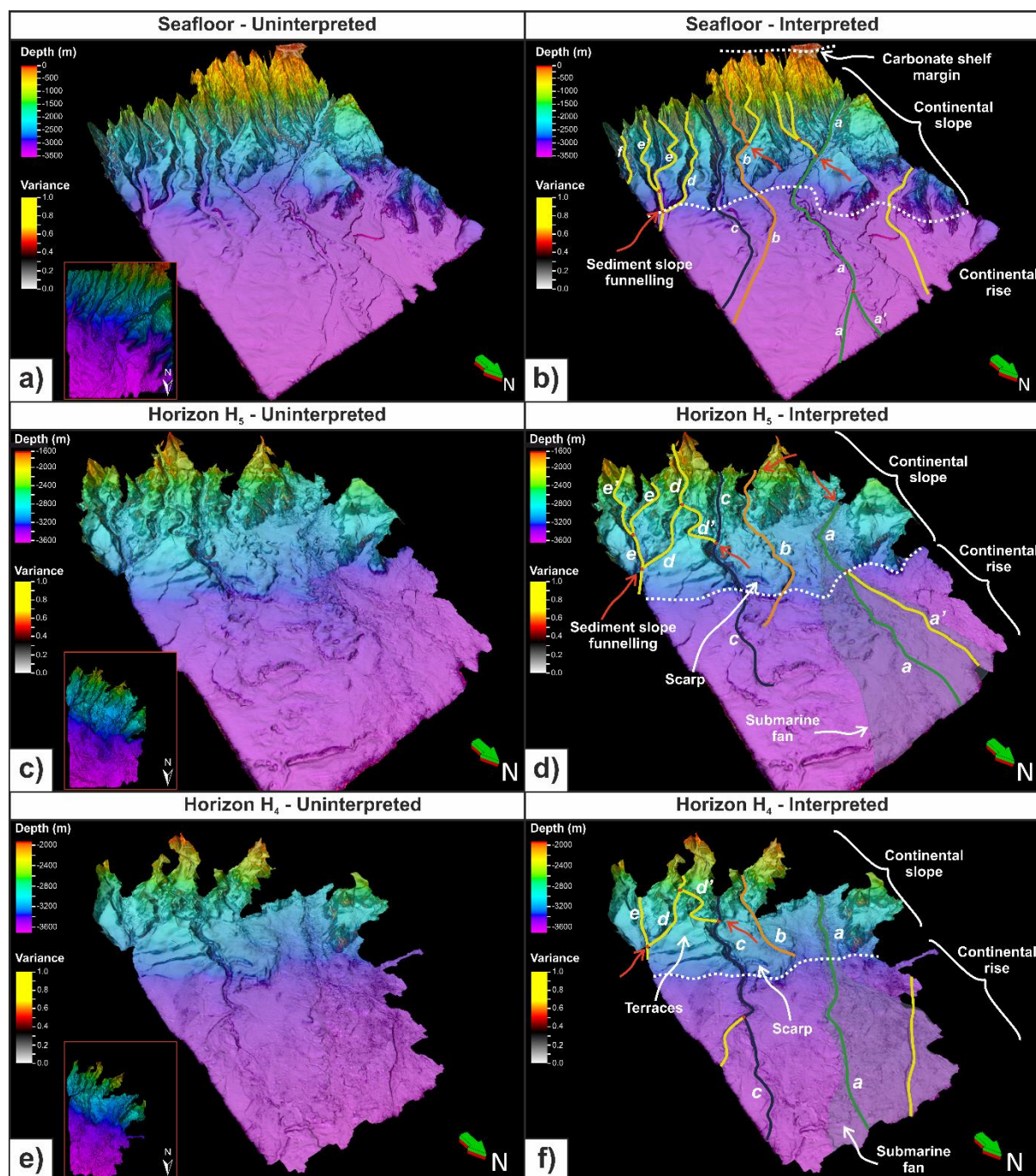
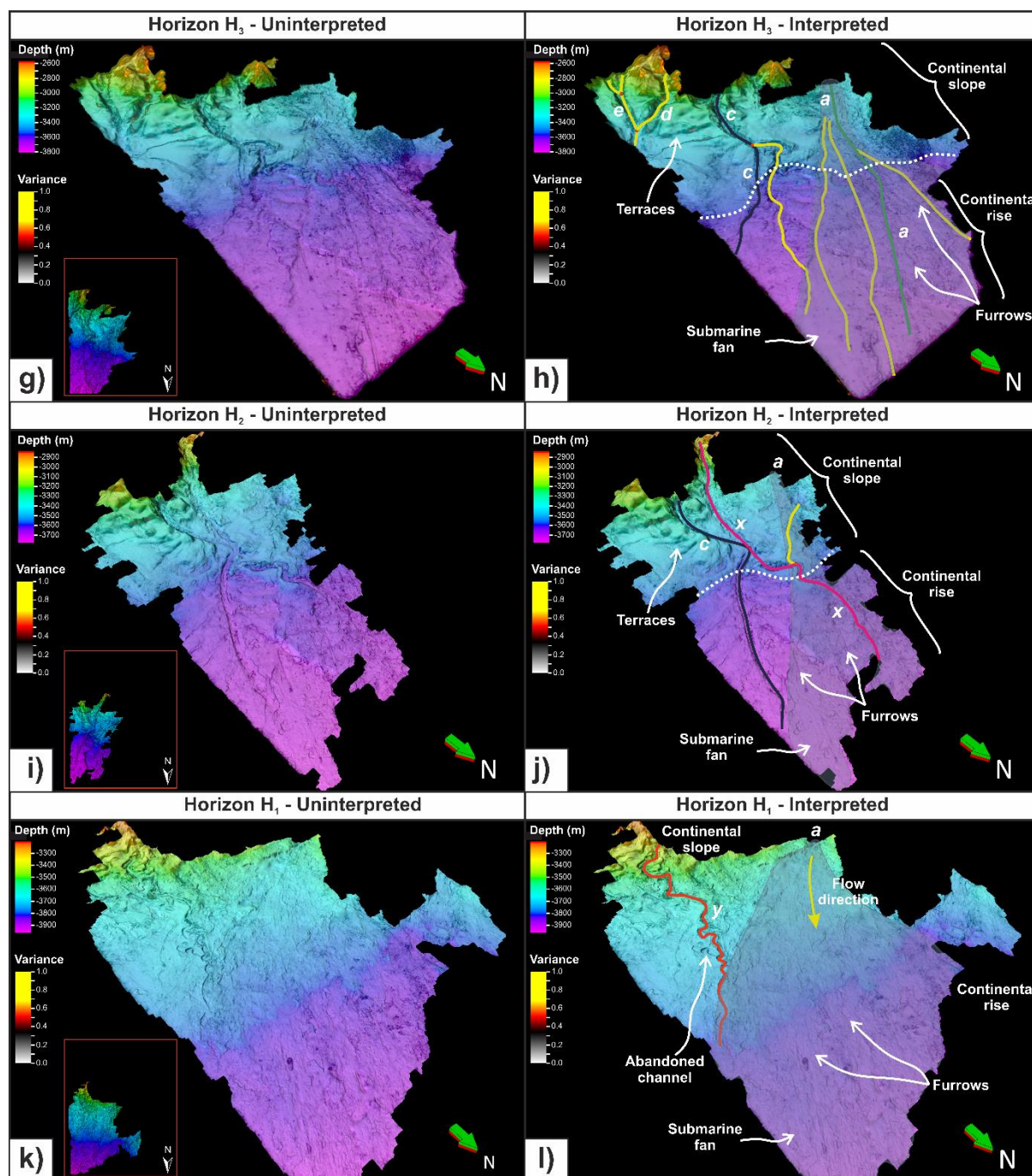


Figure 7. 3D views of blended depth and variance horizon maps at different intervals: Seafloor (a, b), horizon H₅ (c, d), and horizon H₄ (e, f). Uninterpreted (a, c, e) and interpreted (b, d, f) maps are shown, and principal morphological features are highlighted in them, including the channel-levee systems interpreted in this work. Red arrows indicate sediment funnelling points on the continental slope.

1160

FIGURE 7. Continued.



1161

1162 Figure 7. (continued). 3D views of blended depth and variance horizon maps at different
 1163 intervals: horizon H₃ (g, h), horizon H₂ (i, j), and horizon H₁ (k, l). Uninterpreted (g, i, k) and
 1164 interpreted (h, j, l) maps are shown to highlight main morphological features, including the
 1165 channel-levee systems interpreted in this work.

FIGURE 8

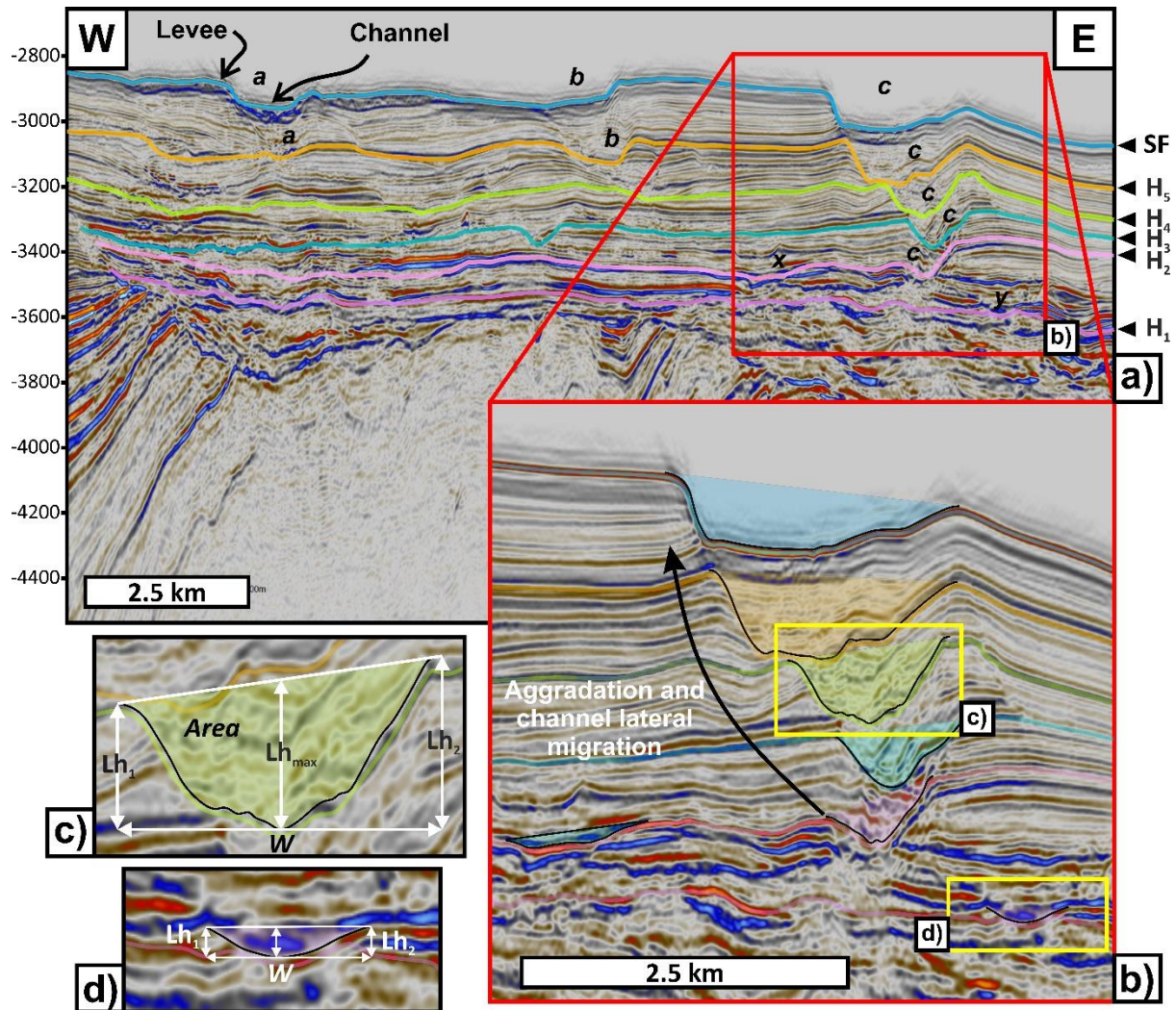
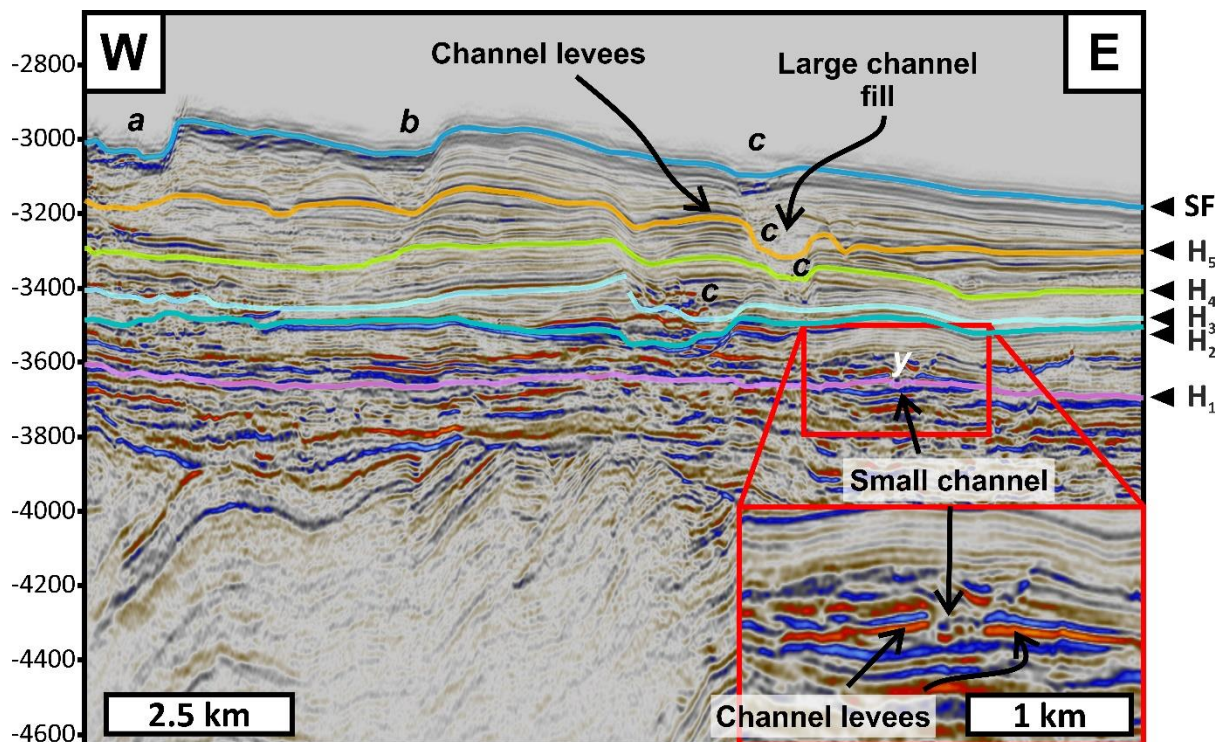


Figure 8. Seismic section showing the channel-levee systems in cross-section and the way in which geomorphic data were measured. Lh_1 and Lh_2 are the levee heights, which is the vertical distance between the deepest points (thalweg) of the channel to the two levee crests. Lh_{max} is the maximum levee height, which is measured as the average height between Lh_1 and Lh_2 , as there is asymmetry in the channels. The parameter W is the channel width, which is measured between the levee crests.

1174

FIGURE 9



1175

1176 Figure 9. Seismic section showing the difference in cross-sectional scale between
 1177 channel-levee systems. Channel y is only about 0.5 km wide and is buried by a low-amplitude
 1178 reflection unit. In contrast, channel c is three to five times wider than channel y and reveals an
 1179 aggradational pattern. Both channels have external levees.

1180

Figure 10

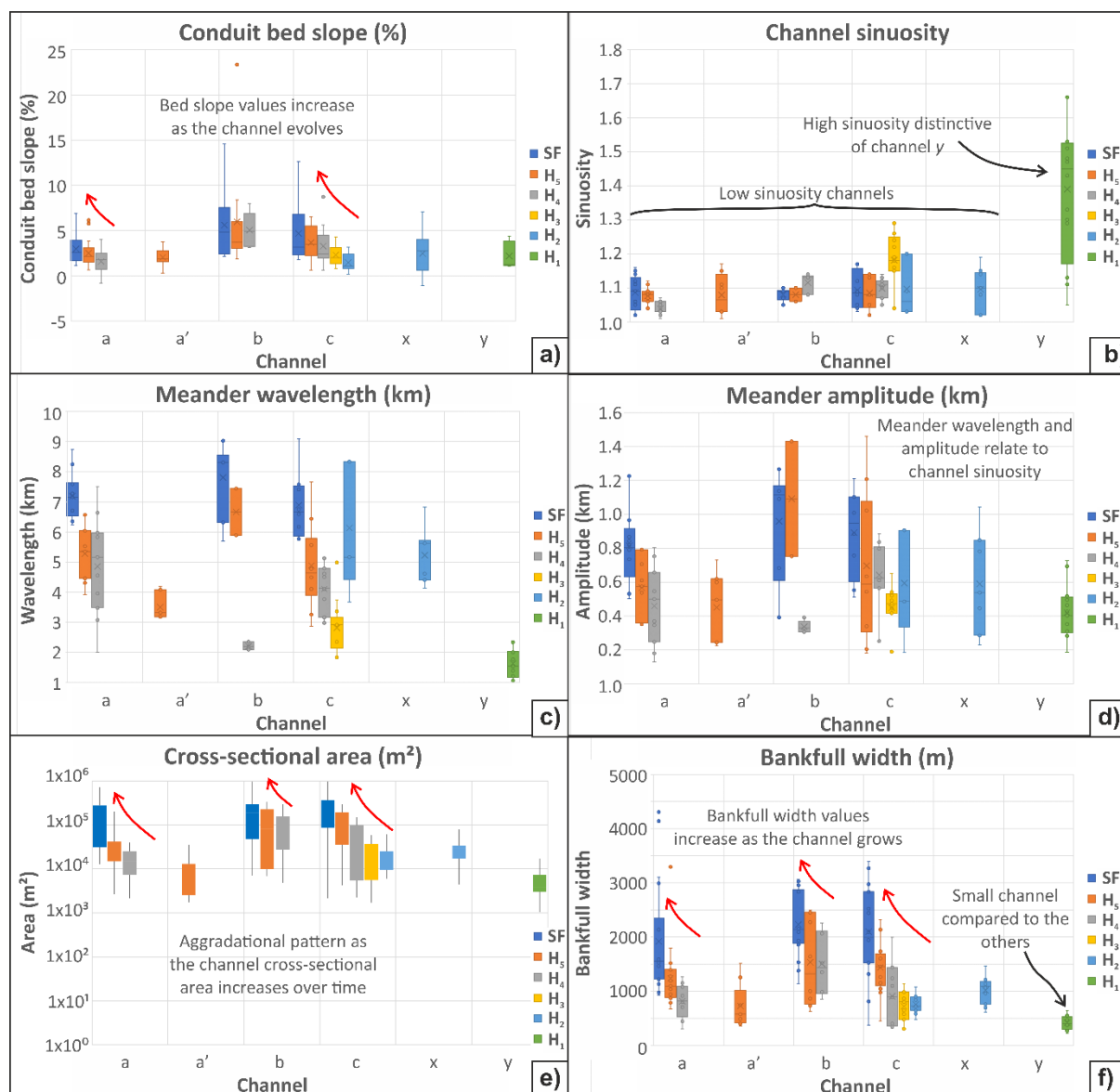
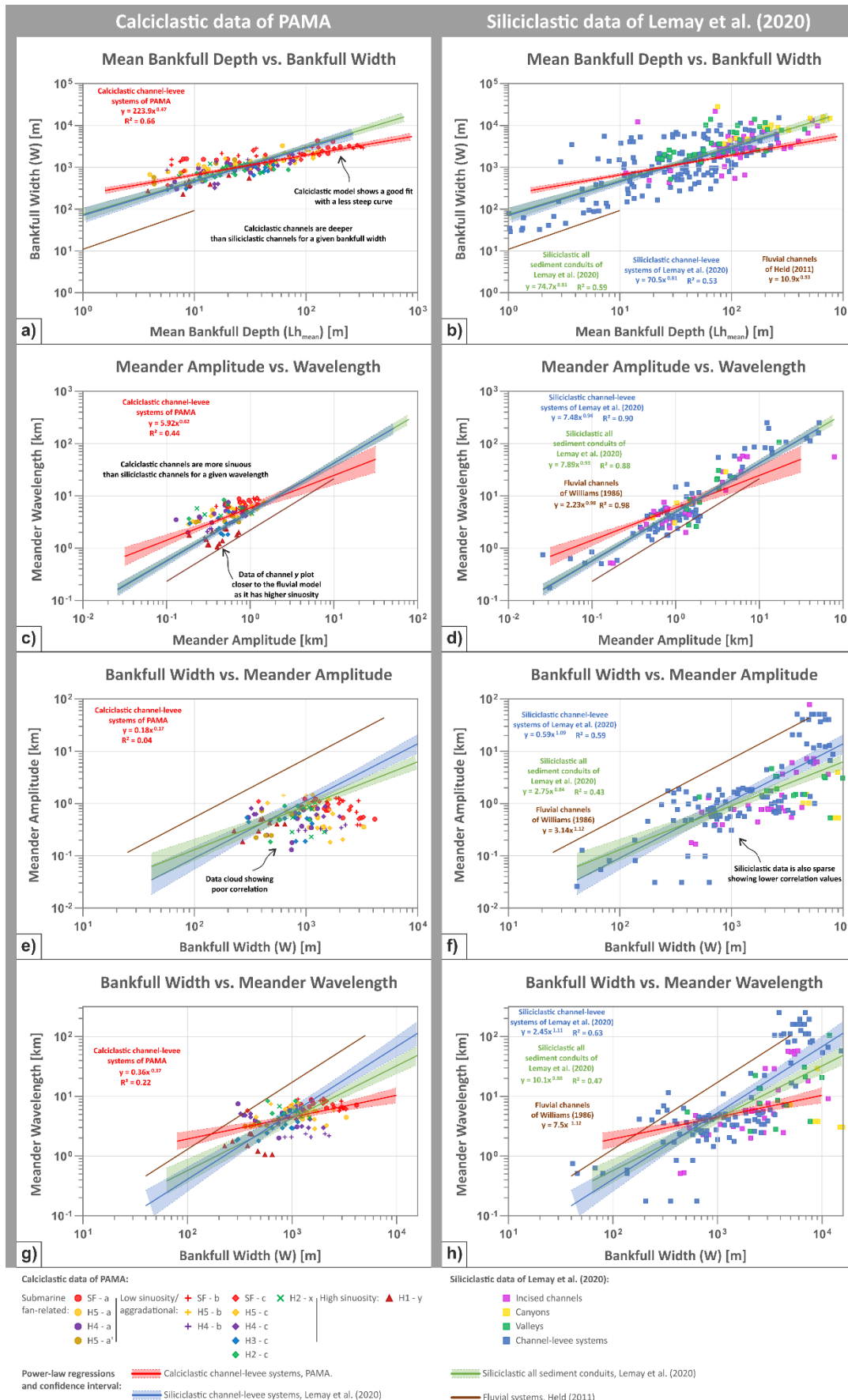


Figure 10. Cross-sectional distribution box plots of the channel-levee systems in the PAMA Basin. a) Conduit bed slope; b) channel sinuosity; c) meander wavelength; d) meander amplitude; e) cross-sectional area; and f) bankfull width.

1187

FIGURE 11

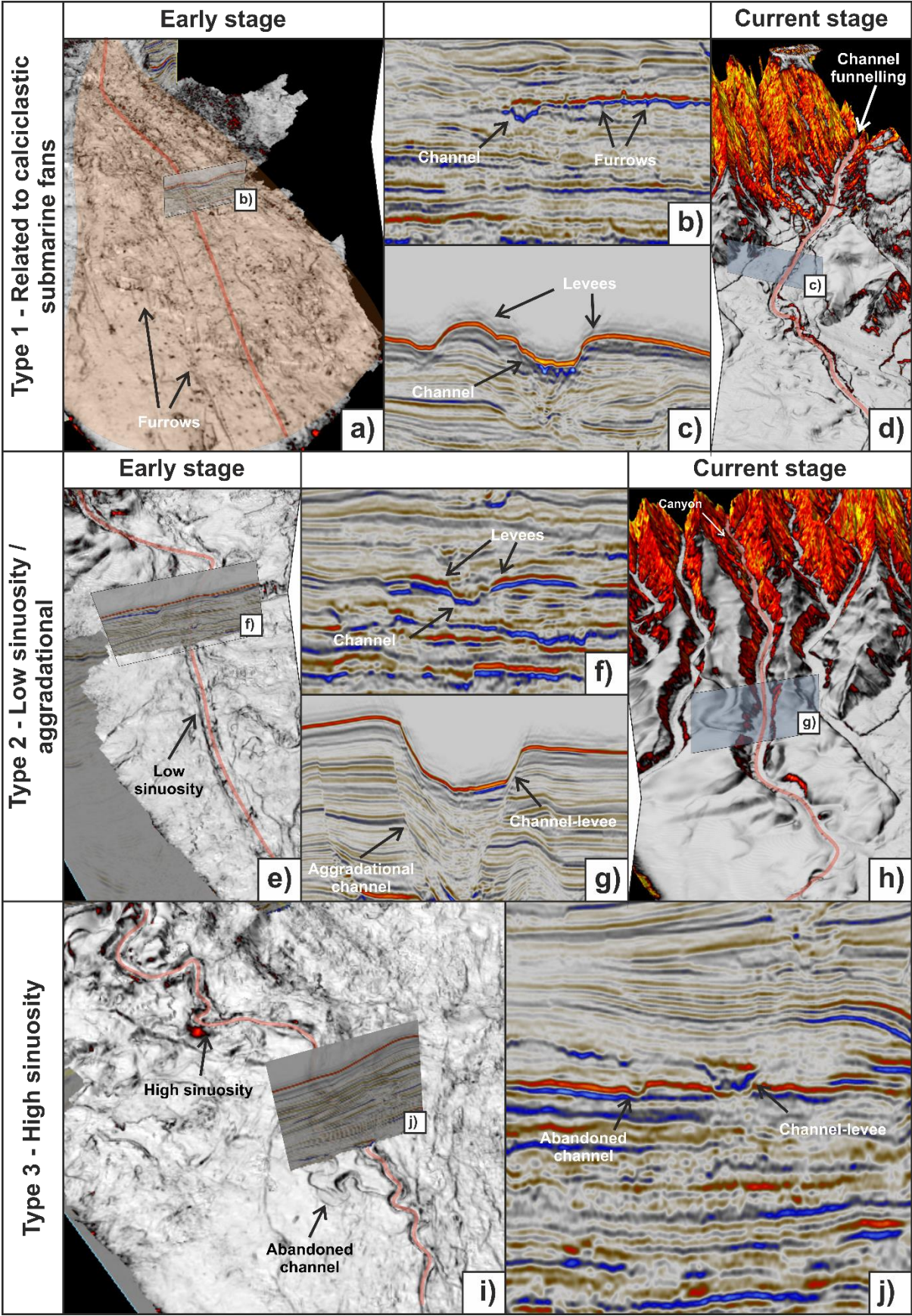


1188

1189 Figure 11. Cross-plots comparing morphometric relationships of calciclastic channel-
1190 levee systems of PAMA and siliciclastic sediment conduits taken from Lemay et al., 2020.
1191 Power-law equations from Williams et al. (1986), Held (2011) and Lemay et al. (2020) are
1192 plotted to compare calciclastic channel-levee systems with the geometries of siliciclastic
1193 submarine and fluvial channels. a and b) Mean bankfull depth (Lh_{mean}) against bankfull width
1194 (W); c and d) meander amplitude vs. meander wavelength; e and f) bankfull width vs. meander
1195 amplitude; and g and h) bankfull width vs. meander wavelength.

1196

FIGURE 12



1197

1198 Figure 12. Summary diagram of 3D seismic data showing the main types of channel-
1199 levee systems occurring in the mixed carbonate-siliciclastic depositional system of the PAMA
1200 Basin.

1201 **14 Data Availability Statement**

1202 The 3D seismic data that support the findings of this manuscript are available from
1203 Polarcus. Restrictions apply to the availability of these data, which were used under license for
1204 this study. 3D seismic data are available with the permission of Polarcus.

1205 The well data that support the findings of this manuscript were provided by the Brazilian
1206 National Agency of Petroleum, Natural Gas and Biofuels (ANP). Restrictions apply to the
1207 availability of these data, which were used under a research licence agreement between ANP
1208 and the University of Goiás, Brazil.